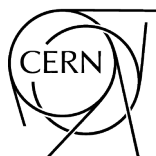


# **LHC fixed target experiments**


**Report from the LHC Fixed Target Working Group  
of the CERN Physics Beyond Colliders Forum**



CERN Yellow Reports: Monographs  
Published by CERN, CH-1211 Geneva 23, Switzerland

ISBN 978-92-9083-573-8 (paperback)  
ISBN 978-92-9083-574-5 (PDF)  
ISSN 2519-8068 (Print)  
ISSN 2519-8076 (Online)  
DOI <https://doi.org/10.23731/CYRM-2020-004>

Copyright © CERN, 2020

 Creative Commons Attribution 4.0

This volume should be cited as:

LHC fixed target experiments: report from the LHC Fixed Target Working Group of the CERN Physics Beyond Colliders Forum  
CERN Yellow Reports: Monographs, CERN-2020-004 (CERN, Geneva, 2020)  
<https://doi.org/10.23731/CYRM-2020-004>.

Corresponding editor: [Stefano.Redielli@cern.ch](mailto:Stefano.Redielli@cern.ch).

Accepted on June 23, 2020, by the [CERN Reports Editorial Board](#) (contact [Carlos.Lourenco@cern.ch](mailto:Carlos.Lourenco@cern.ch)).

Published by the CERN Scientific Information Service (contact [Jens.Vigen@cern.ch](mailto:Jens.Vigen@cern.ch)).

Indexed in the [CERN Document Server](#) and in [INSPIRE](#).

Published Open Access to permit its wide dissemination, as knowledge transfer is an integral part of the mission of CERN.

# LHC fixed target experiments

Report from the LHC Fixed Target Working Group of the CERN Physics Beyond Colliders Forum

C. Barschel<sup>1</sup>, J. Bernhard<sup>1</sup>, A. Bersani<sup>2</sup>, C. Boscolo Meneguolo<sup>3</sup>, R. Bruce<sup>1</sup>, M. Calviani<sup>1</sup>, V. Carassiti<sup>4</sup>, F. Cerutti<sup>1</sup>, P. Chiggiato<sup>1</sup>, G. Ciullo<sup>4</sup>, P. Di Nezza<sup>5</sup>, M. Ferro-Luzzi<sup>1</sup>, A. Fomin<sup>1,6</sup>, F. Galluccio<sup>7</sup>, M. Garattini<sup>1,8</sup>, M. Giovannozzi<sup>1</sup>, C. Hadjidakis<sup>9</sup>, A. Kurepin<sup>10</sup>, N. Kurepin<sup>10</sup>, P. Lenisa<sup>4</sup>, M. Macrì<sup>2</sup>, F. Martinez Vidal<sup>11</sup>, L.M. Massacrier<sup>9</sup>, A. Mazzolari<sup>4</sup>, A. Mereghetti<sup>1</sup>, A. Merli<sup>12</sup>, L. Mether<sup>1</sup>, D. Mirarchi<sup>1</sup>, N. Neri<sup>12</sup>, H. Orth<sup>13</sup>, L.L. Pappalardo<sup>4</sup>, K.L. Poland<sup>1</sup>, B.K. Popovic<sup>1</sup>, K. Pressard<sup>9</sup>, S. Redaelli<sup>1</sup>, P. Robbe<sup>14</sup>, R. Rossi<sup>1</sup>, G. Rumolo<sup>1</sup>, B. Salvant<sup>1</sup>, W. Scandale<sup>1</sup>, E. Steffens<sup>15</sup>, A. Stocchi<sup>14</sup>, N. Topilskaya<sup>16</sup>, and C. Vollinger<sup>1</sup>

<sup>1</sup>CERN, Geneva, Switzerland

<sup>2</sup>Università di Genova and INFN, Genoa, Italy

<sup>3</sup>Università di Padova and INFN, Padua, Italy

<sup>4</sup>Università di Ferrara and INFN, Ferrara, Italy

<sup>5</sup>INFN, Frascati, Italy

<sup>6</sup>NSC Kharkiv Institute of Physics and Technology, Kharkiv, Ukraine

<sup>7</sup>Università di Napoli, Naples, Italy

<sup>8</sup>Imperial College, London, United Kingdom

<sup>9</sup>IPNO, CNRS-IN2P3, Univ. Paris-Sud, Université Paris-Saclay, Orsay, France

<sup>10</sup>Russian Academy of Sciences, Moscow, Russia

<sup>11</sup>Instituto de Física Corpuscular, Universitat de València, Valencia, Spain

<sup>12</sup>Università di Milano and INFN, Milan, Italy

<sup>13</sup>GSI Helmholtz Centre for Heavy Ion Research, Darmstadt, Germany

<sup>14</sup>Laboratoire de l'Accélérateur Linéaire, Université Paris Sud Orsay, Orsay, France

<sup>15</sup>Physics Dept., Friedrich-Alexander-Universität Erlangen-Nürnberg, Erlangen, Germany

<sup>16</sup>Institute for Nuclear Research, Moscow, Russia

## Abstract

Several fixed-target experiments at the LHC are being proposed and actively studied. Splitting of beam halo from the core by means of a bent crystal combined with a second bent crystal after the target has been suggested in order to study magnetic and electric dipole moments of short-lived particles. A similar scheme without the second crystal or other schemes with more conventional solid or gas targets have been proposed to study hadronic matter and the quark-gluon plasma, as well as to provide inputs to cosmic ray physics. Most notably, an upgrade of the existing and already productive LHCb gas target (SMOG), which would make use of a storage cell, has been proposed, designed, and extensively reviewed. The implementation in LHCb of a polarised gas target, based on the storage cell technique, was also discussed, motivated by the nucleon-spin study. The status of these proposals, their technical feasibility and impacts on the LHC machine have been studied in the LHC Fixed Target Working Group of the Physics Beyond Collider forum at CERN. The status and outcome of these studies are presented here.

## Keywords

Physics Beyond Colliders; Large Hadron Collider; fixed targets; internal gas targets; polarised targets; internal solid targets; beam splitting by bent crystals.

## Contents

1	Introduction . . . . .	1
2	Crystal beam splitting for internal fixed-targets and double-crystal implementation . . . . .	2
2.1	Basic concepts, conceptual layout definitions and challenges . . . . .	2
2.2	Status of LHC layout studies on IP8 implementation . . . . .	5
2.3	State-of-the-art of developments for long crystals . . . . .	15
2.4	Feedback from first double-channeling observations at the SPS . . . . .	16
2.5	Relevant LHC machine aspects . . . . .	16
2.6	Alternative layouts under studies: a new layout for the LHC IR3 . . . . .	20
3	Internal solid target and single-crystal implementation . . . . .	22
3.1	Solid target on beam halo . . . . .	23
3.2	Crystal beam splitting on solid target in IP2 . . . . .	23
4	Gaseous targets . . . . .	26
4.1	Types of gases and their impact on the LHC . . . . .	26
4.2	Beam life time and local beam losses . . . . .	28
4.3	Storage cell principle . . . . .	29
4.4	Aperture limitations for storage cells . . . . .	31
4.5	Impedance and wake fields . . . . .	32
4.6	SMOG upgrade (SMOG2) . . . . .	32
4.7	A polarised H/D target at the LHC . . . . .	35
5	Summary and conclusions . . . . .	37

## 1 Introduction

The European Organization for Nuclear Research (CERN) offers a unique accelerator complex that covers beam energies up to 7 TeV at the Large Hadron Collider (LHC) [1], with a variety of beam types (protons, ions). As a part of the Physics Beyond Colliders study at CERN (PBC) [2], a working group on fixed-target physics at the LHC was launched in 2017 to collect concrete proposals from the physics community and evaluate their impact on the LHC. Several proposals have been presented, e.g. the use of bent crystals for separating the beam halo from the core and directing it to an internal target, possibly supplemented with a second bent crystal [3,4] to measure magnetic [5,6] and electric [7,8] dipole moments of short-lived charged baryons, or the use of internal gas targets (possibly polarised) and solid targets for studying hadronic matter, the quark-gluon plasma and also to produce unique cross-section data sets useful for cosmic ray physics models (see for example Refs. [9–13]). The working group addressed the technical feasibility and impact, principally from the perspective of the LHC accelerator, with the aim of producing the present report in the context of the update of the European Strategy for Particle Physics (ESPP). This paper summarizes the outcome of the working group’s studies and outlines possible future studies.

Some of the proposed fixed target experiments build on the experience accumulated in past years in other colliders, such as HERA [14,15], Tevatron [16], and RHIC [17,18]. While studying these cases is certainly pertinent to guide future choices, it is important to highlight aspects specific to the operation of the high intensity beams at the LHC. With a design stored energy of 362 MJ [1], that will nearly be doubled for the High-Luminosity upgrade of the LHC [19] (HL-LHC), collimation and machine or experiment protection constraints, which were less of a concern in previous colliders, must be taken into account early on.

Most fixed target proposals would greatly benefit from re-using an existing detector at the LHC, as this reduces the cost of implementation. The implications for such a hypothetical “host” experiment must be carefully evaluated (operational risks, experiment protection, induced background rates, compatibility of simultaneous operation or sharing of beam time, etc). Some of the proposed scenarios may also have a global effect on all existing LHC experiments, for example in terms of integrated luminosity or induced background. The working group tried to identify possible implications and interferences.

Three main types of fixed target implementations have been considered by the working group. Sketches of these implementations are shown in Fig. 1. The panel (a) shows how the beam halo is extracted from the beam core by use of a channeling bent crystal (crystal-1) and directed towards a solid target located upstream of a forward detector (Fig. 1, panel a). The split beam can be used in conjunction with a second bent crystal (crystal-2) for measuring the magnetic and electric dipole moment of charged baryons or be directed onto a solid target for direct use in a fixed-target physics program. An absorber placed after the detector stops the surviving extracted halo particles. Solid targets can also be directly brought in the vicinity of the beam halo in order to perform physics experiments (Fig. 1, panel b). Here, the targets (whether wires or foils) must be movable in order to approach the beams after stabilization at the required beam energy. The panels (c) and (d) of Fig. 1 show, respectively, how unpolarised (polarised) gaseous targets would be used in front of a forward detector for a fixed target physics program. In the case of a polarised target, additional instrumentation is needed to produce, guide and measure the nuclear polarisation.

This report is organized as follows. The crystal channeling method for beam splitting and fixed-target experiments is addressed in Section 2. Section 3 covers the case of solid targets coupled or not to a crystal for beam halo splitting. The internal gas target options are discussed in Section 4. A summary and conclusions are given in Section 5.

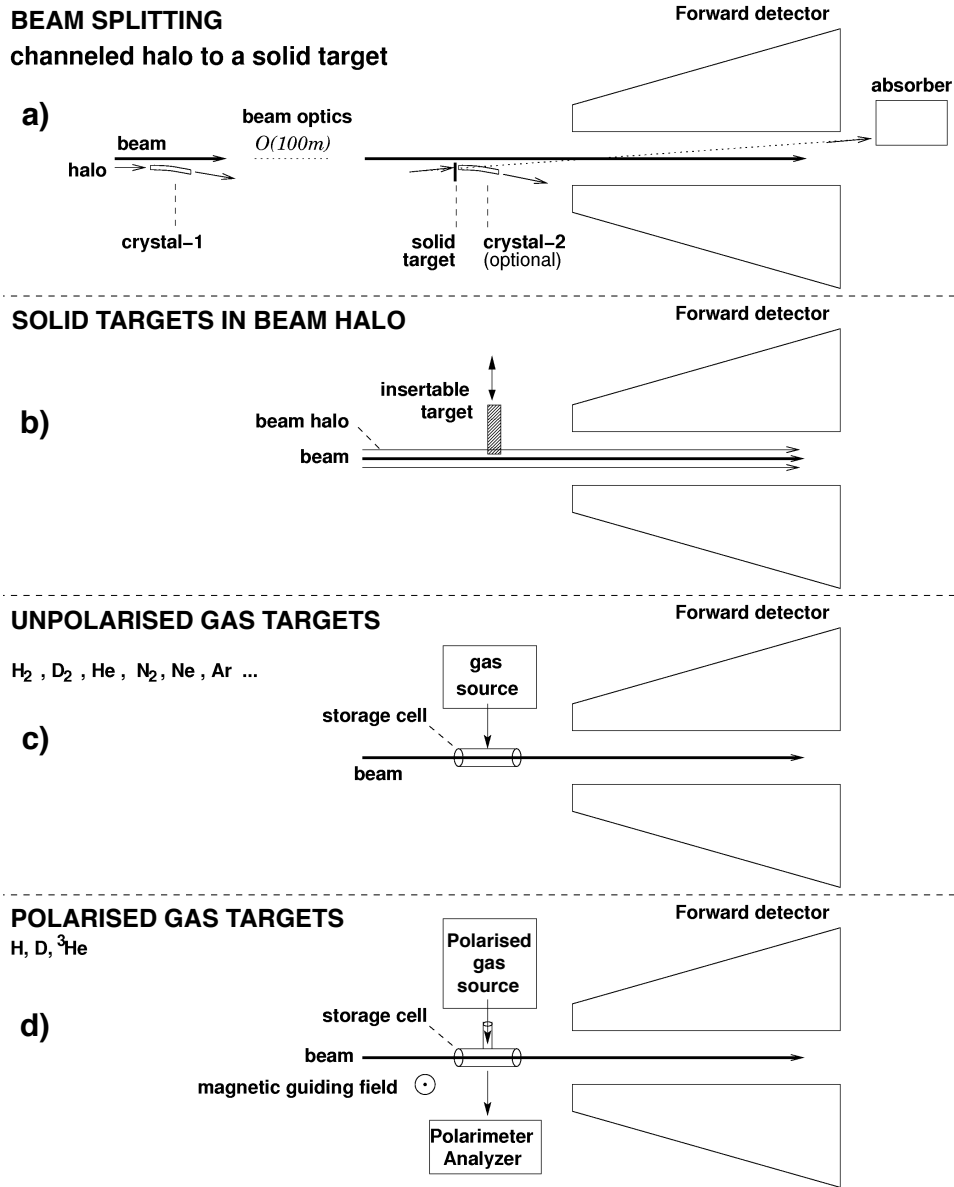


Fig. 1: Sketches of fixed target setups: a) crystal beam splitting for a double-crystal setup or for solid target; b) solid targets in beam halo; c) unpolarised gaseous targets; and d) polarised gaseous targets.

## 2 Crystal beam splitting for internal fixed-targets and double-crystal implementation

### 2.1 Basic concepts, conceptual layout definitions and challenges

In the concept of beam-halo splitting for internal beam targets (Fig. 1, panel a), a bent crystal, similar to the ones presently used for hadron-beam collimation at the LHC [4,20,21], separates from the circulating beam a fraction of the halo that then impinges on an in-vacuum target, safely retracted from the beam core envelope. A specific implementation of this scheme, which we call “double-crystal setup”, was proposed [3] for an experiment in LHCb, to study magnetic dipole moment of baryons [5] (see also Ref. [22]). This idea was extended to search for the electric dipole moment [7, 8]. This scheme is described in detail in this section whereas in Section 3, similar concepts applied to conventional fixed-target assemblies are discussed.

Planar channeling [23] is a coherent phenomenon where positively-charged hadrons are trapped between the crystalline planes of high-purity crystals, with lattice defects inducing dislocation densities

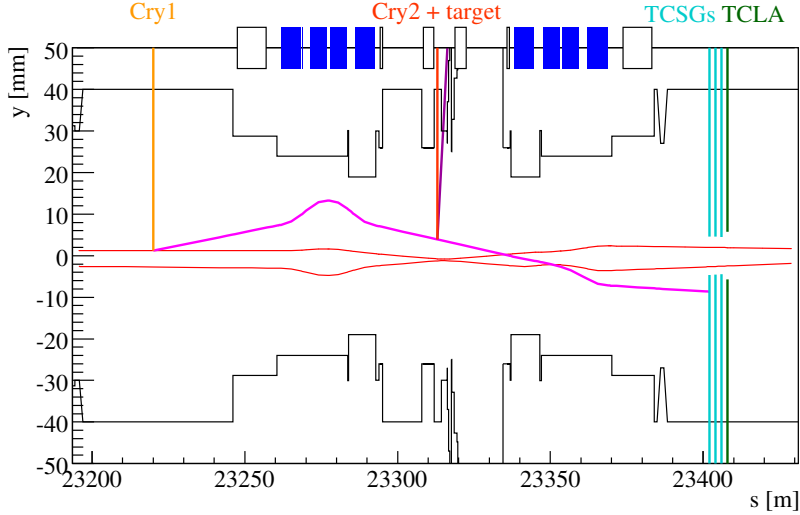


Fig. 2: Implementation of a double-crystal experiment in LHCb, with a first crystal with a  $150 \mu\text{rad}$  bending upstream of the left-side inner triplet (blue boxes) and a second crystal with a  $14 \text{ mrad}$  bending just upstream of the interaction point. New collimators in carbon fibre (cyan bars) and heavy tungsten alloy (dark green) are added downstream [3].

below one per squared centimeter. Bent crystals coherently deflect the particle's trajectories inducing kicks that are equal to the mechanical bending radius of the crystal. For particles in the range above hundreds of GeV, this produces equivalent magnetic fields that are well beyond what can be achieved with conventional magnets. In the halo-splitting scheme, a first crystal, bent to produce kicks of about  $100\text{-}200 \mu\text{rad}$ , separates the beam halo from the circulating beam and induces a separation of several mm between the split halo and the main beam's envelope, at a location where an in-vacuum solid target can be located. The target remains safely retracted from the circulating beam and is only impacted by the split halo.

In the double-crystal setup, the thin target is followed by a second crystal, essentially adjacent to it, with a much larger bending angle in the order of several mrad. The equivalent fields, experienced by particles that are channeled, allow one to study the precession of short-lived baryons that cannot be studied with conventional magnets, as their decay path is too short. Precession of  $\Sigma^+$  in crystals was demonstrated in an extracted-beam experiment at the Tevatron [16]. The implementation in the LHC using crystals would enable a first direct measurement of the dipole moment of the charm baryons  $\Lambda_c^+$  and  $\Xi_c^+$ , and ultimately charged beauty baryons and the  $\tau$  lepton [24, 25]. However the proposed setup is challenging and its feasibility needs to be demonstrated.

A possible layout of this experiment, elaborated for the LHC point 8 (P8), is given in Fig. 2, taken from Ref. [3]. The first crystal, acting on Beam 1, is located upstream of the P8 inner triplet. A bending angle of  $150 \mu\text{rad}$  is sufficient to steer beam halo particles onto a target located  $2.4 \text{ m}$  upstream of IP8<sup>1</sup>. For a first study, a  $5 \text{ mm}$ -long tungsten target was assumed. A second crystal, attached to the target, is used to bend into the LHCb acceptance the decay products of the produced baryons. A much larger bending than for the first crystal, of the order of  $15 \text{ mrad}$ , is required in this case [27]. Further downstream, at least one collimator is needed to dispose in a controlled way of protons and other interaction products that emerge from the first crystal and the target. The detailed layouts are discussed in the next section.

<sup>1</sup>Initial integration studies indicated that a position at a distance of  $2.4 \text{ m}$  from IP8 was available for the installation of the target assembly. A later assessment showed that a closer position at  $1.2 \text{ m}$  from IP8 is actually also accessible which is preferred. While the latter is used in the latest LHCb simulations [27], the former is still used for the loss studies presented in this document. This small shift is not expected to induce significant differences for the loss behaviour.

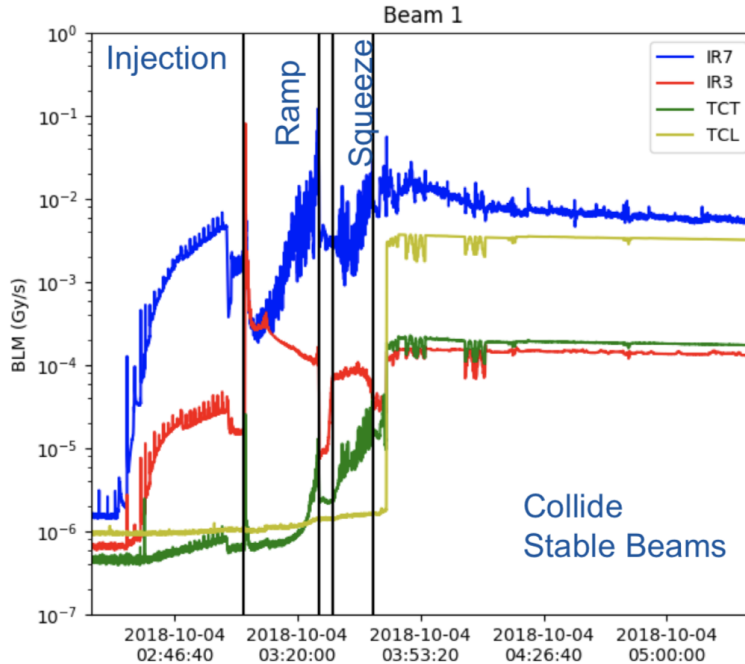


Fig. 3: Example of IR7 losses in a typical fill in 2018. The time for the start of different machine modes is indicated. *Courtesy of B. Salvachua, CERN.*

Clearly, an important design goal in this phase is to assess if such measurement could be done parasitically to the standard LHC operation. For this scenario to be feasible, the first crystal would have to be made part of the present LHC collimation hierarchy, designed to protect the machine from operational losses, and would extract parasitically a portion of the protons that are naturally lost on the betatron collimation system during standard physics data taking. Figure 3 shows an example of beam losses recorded during a typical physics fill in 2018, from injection to collision (“stable beam” mode). In this illustrative example, losses are measured by beam loss monitors at the location of the primary collimators of the LHC betatron collimation system. Transverse losses are by design impacting these primary collimators, which in 2018 were set at 5 beam sigmas (following the notation for the beam sigma  $\sigma = \sqrt{\beta\epsilon}$ , where  $\beta$  is the periodic beta function and  $\epsilon = 3.5 \mu\text{m}$  is the nominal LHC normalized emittance). Losses stabilize in the stable beam mode. The corresponding beam lifetime in this mode is shown in Fig. 4, where the average lifetime in this mode is shown for all the operational years in Run 2. This information is shown for illustration and will be used below for a detailed estimate of achievable losses for the scheme where a crystal is inserted in the transverse collimation hierarchy.

The feasibility of the double-crystal scheme is being studied both from the accelerator and the experiment points of view. There are three main areas of study that are subject of simulation and experimental verification: (1) the feasibility of producing large-angle crystals with the required accuracy and channeling efficiency at the energy of interest; (2) the assessment of realistic rates of protons on target for different LHC operational scenarios; (3) the implementation of the collimation system downstream of LHCb, to be integrated into the present LHC collimation system.

Recently, very promising results towards a feasibility demonstration of the double-crystal concept were obtained by the UA9 collaboration at the CERN SPS, where a complete double-crystal test stand has been set up [28]. In 2017, the double channeling was demonstrated for the first time, by placing a crystal into the halo channeled by a first crystal in a setup equivalent to that proposed for the experiment, although with the second crystal at lower bending angles and still without target [29]. In 2018, additional measurements were carried out in the SPS by adding to the setup a target, made of a movable, 3 mm thick tungsten block, upstream of the second crystal. For the first time, leading to the first observation of



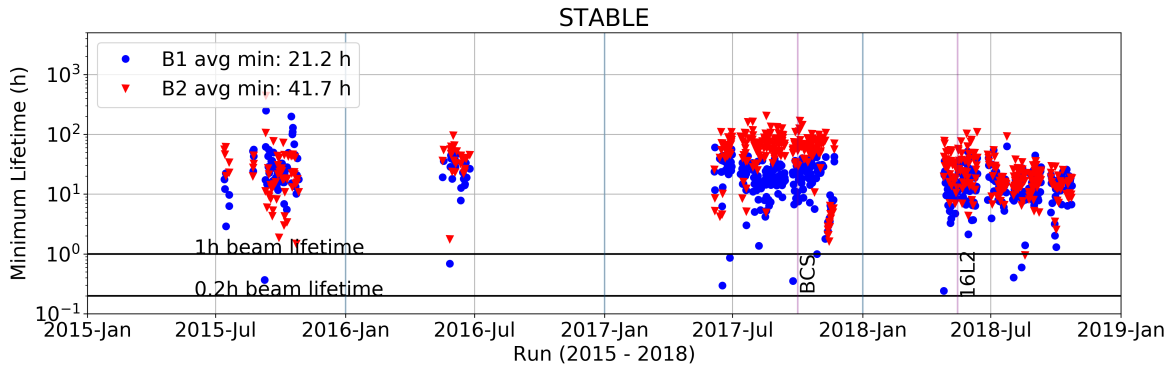


Fig. 4: Minimum beam lifetime recorded in the stable beam mode during the operational years of Run 2. *Courtesy of B. Salvachua, CERN.*

channeling of products created by the interaction of the channeled halo with the target.

For all considered implementations of the double-crystal scheme, it is essential to achieve a very good channeling performance with the second crystal that generates the spin precession of the  $\Lambda_c^+$  produced at the target. The crystal bending angle must be compatible with the LHCb detector acceptance, larger than 10 mrad, and induce sufficient spin precession to the channeled particles. Channeling performance of such crystals can only be assessed satisfactorily in dedicated beam tests with hadron beams, since the present simulations tool are benchmarked only for angles up to milli-rad at the energies of interest. Experimental validation of long crystals was set as a key milestone before relying on the double-crystal setup for future experiments. This led to important new measurements in 2018, carried out by two independent teams that are now being analysed in detail. The current status will be briefly reported in Section 2.3 of this chapter.

## 2.2 Status of LHC layout studies on IP8 implementation

In this section, an optimized layout for a double-crystal experiment in IR8 for Beam 1 is presented. The impact on the machine, with emphasis on collimation aspects and beam losses, is discussed. The scenario of a vertical setup – i.e. with crystal and target inserted in the beam along the vertical plan, from the top – is considered to avoid concerns related to fast losses in case of asynchronous beam dump failures, which only affect the horizontal plane. The first crystal is inserted as a secondary collimator in the transverse hierarchy of the betatron collimation system that involves primary and secondary collimators in IR7, and tertiary collimators in all experiments. The achievable rates of protons on target for this configuration are presented, assuming operational losses in stable beams as observed in the 2018 LHC run. For this study, we consider a parasitic scenarios with the goal to make this setup compatible with the operation at high intensity for luminosity production in ATLAS and CMS. In particular, we take as an input that the IR8 optics remains the same as for the standard LHCb operation, as any other change would entail lengthy dedicated commissioning setups.

### 2.2.1 General considerations on design criteria and IR8 layout

The main goal of the layout optimization is to maximize the number of protons on target (PoT) while minimizing the impact on the LHC operation, specifically the losses on superconducting magnets around the ring. Similar design approaches as the ones applied for the definition of the crystal collimation system of IR7 [20] were followed. An important specific constraint in IR8 is the limited available space. Although this work does not include a dedicated integration study, all known constraints from the present IR8 space occupancy were taken into account for the choice of positions of the movable elements. Given the space constraint from present hardware, the choice of optimum location of the first crystal is chosen

Table 1: Installation position and main features of the proposed experimental layout in IR8. All the components act on the vertical plane. The position if IP8 is 23315.4 m.

Name	$s$ from IP1 [m]	Bending [ $\mu$ rad]	Length [cm]	Mat.	Bending planes
Cry <sub>1</sub>	23220	150	1.2	Si	110
Target	23313	-	0.5	W	-
Cry <sub>2</sub>	23313	14000	7	Si	110
TCSG.A4R8.B1	23402	-	100	CFC	-
TCSG.B4R8.B1	23404	-	100	CFC	-
TCSG.C4R8.B1	23406	-	100	CFC	-
TCLA.A4R8.B1	23408	-	100	W	-

to enhance the displacement at the target while minimizing the beam divergence.

For LHC operation at high intensities, additional collimators need to be added downstream of IP8 to dispose of the channeled halo that emerges from the target and to dispose of out-scattered protons. Optimizing the location for such collimators calls for an installation at the closest location where the betatron phase advance from the first crystal is about  $\pi/2$ . Smaller beam sizes at the collimators are also favoured because they allow closer settings and thus a better efficiency in intercepting particles emerging from crystal and target. These two parameters – phase difference and transverse settings – define the angular cut made by the absorber. For convenience, this is typically expressed as the minimum kick for particles out-scattered at the crystal that are still intercepted by the downstream collimators.

Between the first crystal and the absorber, the trajectory of channeled halo particles must remain at least 4 mm apart from the geometrical LHC aperture, following the guidelines from the LHC Technical Design Report [1]. Detailed aperture calculations, with a proper accounting of relevant errors on optics, aperture, orbit, etc., shall be performed at a later stage. One also requires a distance between the target and the circulating beam envelope of 4 mm, which defines the minimum bending angle of the first crystal. This retraction ensures that the target is not intercepting significant beam halo. It can be demonstrated that, for the operational scenarios discussed below, approaching the target further does not bring significant benefits. The possibility to optimize the first crystal could be considered in the future.

The choice of the vertical plane is made in order to avoid the machine protection constraint that horizontal movable devices must be compatible with the asynchronous beam dump [35], and in general must sustain losses that are produced every time when a beam dump is triggered. It can happen that the beam-dump kickers are not fired synchronously with respect to the abort gap. A portion of beam, well-above the damage limit of metals, is kicked wrongly and can impinge on horizontal aperture restrictions. In this setup, a fraction of particles could be directly extracted on the target causing a burst of dissipated energy in LHCb. This can only be avoided by taking sufficient margins in the horizontal aperture (typically, above 12-15  $\sigma$  unless specific optics constraints are defined). It will be shown in the following that such settings would not allow a significant rate of PoT. This failure mode does not apply for the vertical restrictions, opening the possibility to approach the beam further in this plane. We assume that the crystal is moved into the beam from top, assuming the design of the vertical goniometers in IR7 (see below).

The double crystal layout in IR8 is shown in Fig. 2 and the relevant parameters are summarized in Table 1. The first crystal (Cry<sub>1</sub>) produces a bending  $\theta_b^{\text{Cry}_1} = 150 \mu\text{rad}$ . The average trajectory of channeled particles is showed in magenta. The crystal length is  $l^{\text{Cry}_1} = 1.2 \text{ cm}$ , which was chosen to have a bending radius  $R = 80 \text{ m}$ , the same as the present crystals for collimation installed in IR7, following the approach described in Ref. [20].

In the simulations of beam losses, the target is placed immediately upstream of the LHCb de-

Table 2: LHC operational parameters in 2018 at End of Squeeze.

IP	$\beta^*$ [cm]	Crossing angle [ $\mu$ rad] (plane)	Sep. [mm] (plane)	IP disp. [mm] (plane)
1	30	160 (V)	-0.55 (H)	0
2	1000	200 (V)	1 (H)	-2 (V)
5	30	160 (H)	0.55 (V)	-1.8 (V)
8	300	-250 (H)	-1 (V)	0

tector at about 2.4 m from IP8. Later studies indicated as optimum position a location at 1.16 m from LHCb [27], but the impact on beam losses from this change is expected to be negligible. It is important to be as close as possible to the Vertex Locator (VELO) [36] to obtain the best resolution on the decay vertex. The target is made of tungsten and is 5 mm long [6, 37]. Further optimizations are possible but not studies in detail here. The second crystal (Cry<sub>2</sub>) produces a bending of  $\theta_b^{\text{Cry}_2} = 14$  mrad and has a length of  $l^{\text{Cry}_2} = 7$  cm [8]. Both crystals are made of silicon that has established and proven purity, typically below 1 defect per cm<sup>2</sup>. If Germanium crystals at large bending were proved to be feasible, a further gain between 2 and 4 could be obtained [27, 38].

Beam halo particles that do not interact with the target+Cry<sub>2</sub> assembly are intercepted by 4 double-sided LHC-type collimators. The first 3 are made of 1 m long Carbon-Fiber-Carbon composite jaws as the present TCSGs, while the last one is made of 1 m long tungsten jaws (TCLA design) to maximise absorption [39]. This is a performance-oriented assumption adopted for the first assessment in simulations, which does not take into account cost and resource considerations. These aspects shall be reviewed at a later stage. Detailed integration in this region where beams share a common beam pipe should also be studied. The proposed longitudinal positions optimize the angular cut on protons out-scattered by the Cry<sub>1</sub>. Protons that acquire an angular deflection  $> 60$   $\mu$ rad by the Cry<sub>1</sub> are intercepted if the TCSG collimators are set at  $10 \sigma$  (minimum setting allowed to respect collimation hierarchy). This setting is compatible with the betatron hierarchy of IR7.

It is noted that this setup is only on one side of the beam, as initially proposed in Ref. [40], contrary to what was proposed in Ref. [8]. This choice has no critical impact on the studies carried out here, and simplifies operational aspects and the overall complexity of the apparatus. Taking into account the multi-turn dynamics, our study indicates that the improvement on PoT rates from doubling the devices by installing them at both sides is minor. If the Cry<sub>1</sub> were to be used as primary collimator, it would intercept all particles diffusing out of the core, thus, a second, symmetric apparatus would not bring an increase of PoT rates. For retracted Cry<sub>1</sub> settings the impact was minor for the optics of 2018 studied here.

### 2.2.2 Machine configuration and operational losses

An extensive simulation study was carried out to assess the expected performance of the layout proposed. The main goal is the evaluation of the loss pattern around the entire LHC ring, to be compared to the collimation losses in the present operational configuration. This is important in order to define operational scenarios that respect standard criteria for beam losses. Ideally, if there was no impact on ring losses when inserting Cry<sub>1</sub> and target, one could perform measurements during standard physics operations. This operational mode is defined as *parasitic*. In practice, the presence of additional losses poses limits to the total beam intensity and/or to the closest settings of the apparatus, which directly translated in a limitation of the achievable rates of PoT.

An example of simulated loss maps with 2018 operational settings is shown in Fig. 5. Losses on superconducting magnets, warm elements and collimators are indicated as cold, warm and collimator, respectively. It is clearly visible that the Dispersion Suppressor in IR7 (IR7-DS) is the limiting location of the whole ring in terms of cleaning efficiency, i.e. where the highest cold losses occur. These magnets

Table 3: LHC collimation settings in 2018.

Coll. Family	IR	Settings [ $\sigma$ ]
TCP/TCSG/TCLA	7	5.0 / 6.5 / 10
TCP/TCSG/TCLA	3	15 / 18 / 20
TCTP	1 / 2 / 5 / 8	8.5 / 37 / 8.5 / 15
TCL	1 / 5	OUT
TCSP/TCDQ	6	7.4 / 7.4

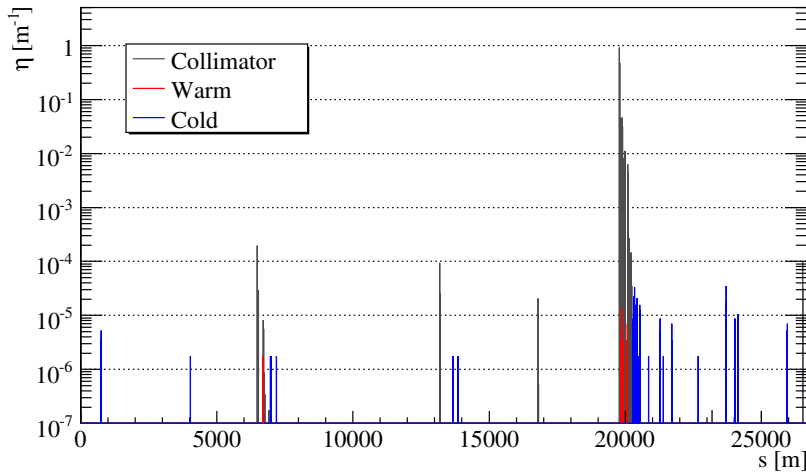


Fig. 5: Reference collimation losses around the ring for vertical losses of beam 1, with nominal machine configurations and collimator settings at 6.5 TeV in 2018 reported in Tables 2 and 3, respectively. The simulation limit of 1 proton lost in the machine aperture corresponds to  $1.8 \times 10^{-6} \text{ m}^{-1}$  in a 10 cm longitudinal bin.

risk to quench in case of high beam losses. To first approximation, we assume that losses induced by the  $\text{Cr}_{Y1}$  and target setup must remain below these levels of losses, i.e. below about  $2 \times 10^{-5} \text{ m}^{-1}$ , as a pre-requisite to allow parasitic data taking with the double-crystal setup <sup>2</sup>.

The beam loss pattern obtained when placing the  $\text{Cr}_{Y1}$  at  $5 \sigma$ , like primary collimators, is shown in Fig. 6. The target sits at about 4 mm from the central beam orbit, as in Fig. 2. The aperture of new TCSGs and TCLA collimators in IR8 is  $10 \sigma$  and  $13 \sigma$ , respectively, in order not to interfere with the multi-turn betatron cleaning process. This layout and setting lead to losses that are not compatible with high-intensity operations by the criteria defined above, i.e. they do not remain lower than collimation losses around IR7. Very high cold losses are recorded in the arc 81 that are well above the IR7-DS levels. It is noted that the IR7 collimation system will be upgraded as a part of the HL-LHC project [19] to remove loss limitations to the total beam current from the IR7-DS losses, by adding local collimators in the DS. This upgrade will take place in Long Shutdown 2 (LS2).

We conclude therefore that it is not possible to use this layout and settings for parasitic operation with a full machine. One can also use these simulation results to establish upper limits for the dedicated operational mode. Since the highest cold peaks in Fig. 6 are up to 10 times larger than in the reference case of Fig. 5, one can expect that circulating beam intensities about 10 times smaller than the nominal

<sup>2</sup>In case of significant losses occurring at other cold locations around the ring, a complete assessment must be done, including also local energy deposition studies at the affected elements. This is not done yet in IR8. Collimation losses at the IR7-DS are well known and studied through dedicated quench tests with beam, but this is not the case at any other ring location.

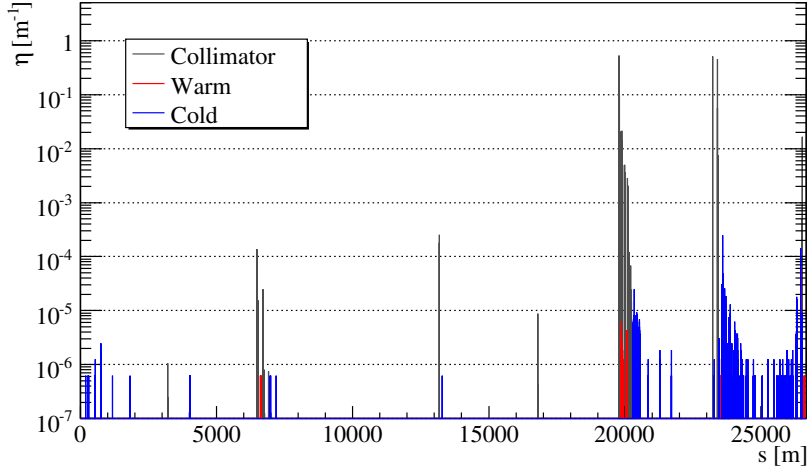


Fig. 6: Simulated beam loss pattern for the double-crystal layout with  $\text{Cry}_1$  at  $5\sigma$ . The simulation limit of 1 proton lost in the machine aperture corresponds to  $1.8 \times 10^{-6} \text{ m}^{-1}$  in a 10 cm longitudinal bin. Losses downstream of IR8 exceed by far the levels of  $\approx 2 \times 10^{-5} \text{ m}^{-1}$  recorded in the IR7-DS that are considered tolerable with the present machine.

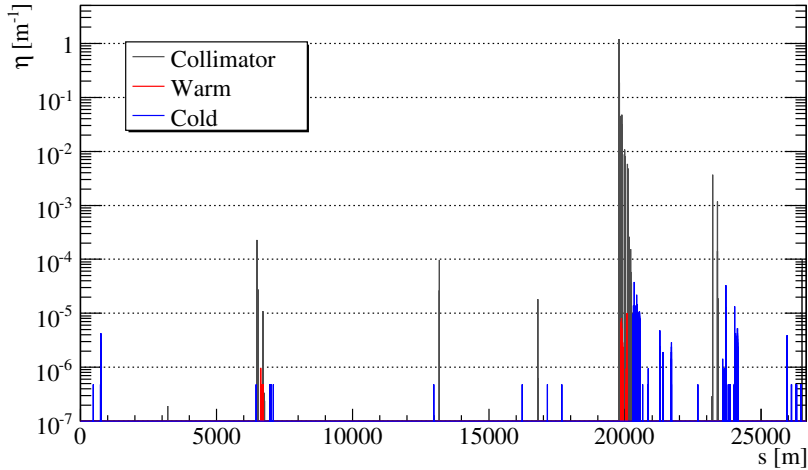


Fig. 7: Simulated beam loss pattern for the double-crystal layout with  $\text{Cry}_1$  at  $6\sigma$  ( $1 \text{ p} = 4.8 \times 10^{-7} \text{ m}^{-1}$ ).

LHC, e.g. 200-250 nominal bunches, could be tolerated for the same loss assumption. At this stage, scenarios where the  $\text{Cry}_1$  risks to become a primary collimator are excluded, and adequate setting margins must be foreseen to avoid that such scenario occurs.

A significant reduction of losses is obtained for larger aperture of the  $\text{Cry}_1$ . Simulations with  $\text{Cry}_1$  settings from  $6\sigma$  to  $8\sigma$  in steps of  $1\sigma$  were carried out. A similar loss pattern as standard operational performance, in terms of cold losses, is obtained when the  $\text{Cry}_1$  is at  $6\sigma$ , as can be seen from Fig. 7. Thus, *parasitic* operations with  $\text{Cry}_1$  at  $6\sigma$  may be possible from the collimation point of view.

### 2.2.3 Expected protons on target

The expected flux of protons on target are calculated for a scenario where the data taking is done fully parasitically to the high-intensity luminosity production. We assume that, after bringing beams in collision, the experimental apparatus of IP8 is put in place and the first crystal extracts onto the target a

Table 4: Fraction of simulated protons that hit the Cry<sub>1</sub> in IR8 and relative channeling efficiency, together with integrated proton flux in a 10 h fill with 200 h beam lifetime. Note that, as discussed in the text, the scenario at 5  $\sigma$  assumes a circulating beam intensity of 250 bunches, so it is not achievable if not in a dedicated mode of operation. The assumed number of bunches,  $N_b$ , is also given for the other configurations considered for a parasitic running mode.

Cry <sub>1</sub> setting [ $\sigma$ ]	$N_b$	$\frac{N_{\text{imp}}^{\text{Cry}_1}}{N_{\text{sim}}}$	$\varepsilon_{\text{CH}}^{\text{Cry}_1}$	$\int_{10\text{h}} \text{PoT}(t) dt$ [p]
5	255	0.67	0.74	$2.7 \times 10^{11}$
6	2556	$3.1 \times 10^{-3}$	0.41	$6.9 \times 10^9$
7	2556	$3.5 \times 10^{-4}$	0.56	$1.1 \times 10^9$
8	2556	$5.3 \times 10^{-5}$	0.36	$1.0 \times 10^8$

portion of the beam halos generated from primary protons impinging on the IR7 primary collimators (see Figs. 3 and 4) and reaching IR8 through the multi-turn cleaning mechanism. The expected rate of  $\text{PoT}(t)$  can be expressed as:

$$\text{PoT}(t) = \frac{1}{2} \frac{I(t)}{\tau_b} \exp\left(-\frac{t}{\tau_b}\right) \frac{N_{\text{imp}}^{\text{Cry}_1}}{N_{\text{sim}}} \varepsilon_{\text{CH}}^{\text{Cry}_1}, \quad (1)$$

where  $\frac{I(t)}{\tau_b} \exp\left(-\frac{t}{\tau_b}\right)$  is the beam loss rate that is expressed for a given beam lifetime  $\tau_b$  and circulating intensity  $I(t)$ ; the factor  $\frac{1}{2}$  is assumed as sharing between horizontal and vertical loss planes [42];  $\frac{N_{\text{imp}}^{\text{Cry}_1}}{N_{\text{sim}}}$  is the fraction of simulated protons that hit the Cry<sub>1</sub>, and  $\varepsilon_{\text{CH}}^{\text{Cry}_1} = \frac{N_{\text{CH}}^{\text{Cry}_1}}{N_{\text{imp}}^{\text{Cry}_1}}$  is the channeling efficiency of Cry<sub>1</sub> (i.e. fraction of impacting protons trapped between crystalline planes for the entire path in the crystal). Note that the factor  $\frac{N_{\text{imp}}^{\text{Cry}_1}}{N_{\text{sim}}}$  tends to 1 for crystal settings close to that of the primary collimators, but becomes much smaller when the crystal is at secondary or tertiary collimator settings and intercepts only a small fraction of the circulating beam halo. In this formalism, the lifetime  $\tau_b$  is used to measure primary beam losses that occur in IR7 (beam particles impinging on the primary collimators). This is a complex function of time that depends on various machine parameters and configuration changes during the collision process. The total intensity  $I(t)$  is dominated by the collisions in all experiments<sup>3</sup> evolves in time approximately as:

$$I(t) = I_{\text{tot}} \exp\left(-\frac{t}{\tau_{\text{BO}}}\right), \quad (2)$$

where  $I_{\text{tot}}$  is the total stored intensity at the beginning of the fill, while  $\exp\left(-\frac{t}{\tau_{\text{BO}}}\right)$  takes into account the intensity decay due to burn-off from collisions in all IPs (with  $\tau_{\text{BO}} \sim 20$  h [43]). A summary of some critical factors in Eq. (1), as obtained in simulations with different settings of Cry<sub>1</sub>, is given in Table 4. Assuming a conservative beam lifetime of  $\tau \sim 200$  h, which is inferred from the operational experience in 2018 [44], the achievable instantaneous and integrated PoT(t) during one fill are shown in Fig. 8. More aggressive running conditions in terms of dynamic aperture can lead to a reduced beam lifetime and increased losses in IR7, which are normally avoided in order to maximize the number of protons lost by burn-off. The PoT values integrated in 10 h, assumed as a typical LHC fill length, are reported in Table 4. The maximum  $I_{\text{tot}}$  stored in 2018 was of 2556 bunches with about  $1.1 \times 10^{11}$  protons per bunch, i.e. about  $2.8 \times 10^{14}$  protons injected [44]. This initial intensity is scaled down by a factor 10 for Cry<sub>1</sub> setting of 5  $\sigma$ , as explained previously to allow *dedicated* operations.

<sup>3</sup>Note that collision losses mainly occur locally around the IPs with a minimum leakage to IR7.

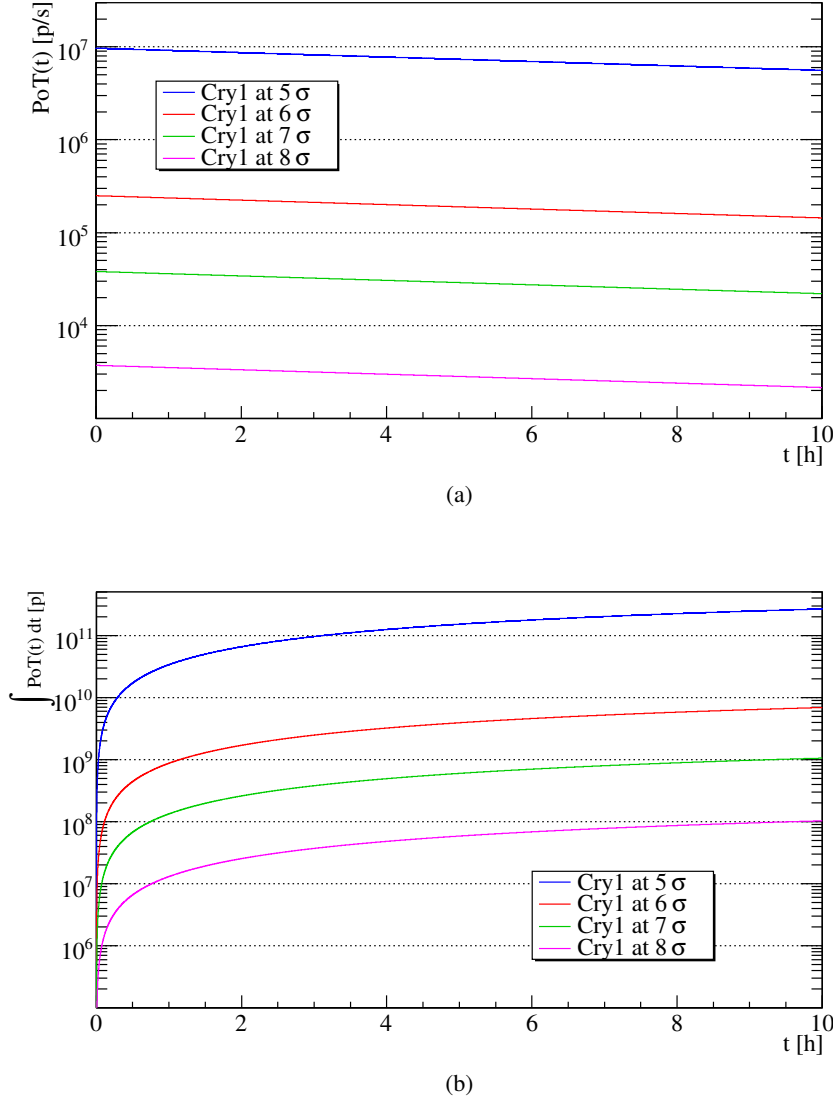


Fig. 8: Expected instantaneous (a) and integrated (b) proton fluxes for different settings of Cry<sub>1</sub> in IR8 during a 10 h fill with 200 h beam lifetime.

#### 2.2.4 Preliminary assessment of $\Lambda_c$ production for a perfect crystal 2

Let us define the efficiency of  $\Lambda_c^+$  channeled by the Cry<sub>2</sub> as:

$$\varepsilon_{\text{CH}}^{\Lambda_c}(E) = \frac{N_{\text{CH}}^{\Lambda_c}(E)}{N_{\text{imp}}^{\Lambda_c}(E)} \exp(-l_{\text{Cry}_2}/c\gamma\tau_{\Lambda_c}), \quad (3)$$

where  $N_{\text{CH}}^{\Lambda_c}(E)$  represents the number of  $\Lambda_c$  that are trapped and remain in channeling for the full crystal length without considering their decay,  $N_{\text{imp}}^{\Lambda_c}(E)$  is the number of impacting  $\Lambda_c$ ,  $l_{\text{Cry}_2}$  is the length of Cry<sub>2</sub> and  $c\tau_{\Lambda_c} = 59.9\mu\text{m}$  [45] is the decay length of the  $\Lambda_c$  baryon. The distribution of  $N_{\text{imp}}^{\Lambda_c}(E)$  was obtained using the PYTHIA8.240 event generator, starting from the impacting distribution of protons on the target, coming from Cry<sub>1</sub> and simulated with the multi-turn simulations described in the previous section. The distribution of  $\Lambda_c$  obtained for 6.5 TeV protons on target is shown in Fig. 9. The efficiency of  $\Lambda_c$  channeled by the Cry<sub>2</sub> is shown in Fig. 10.



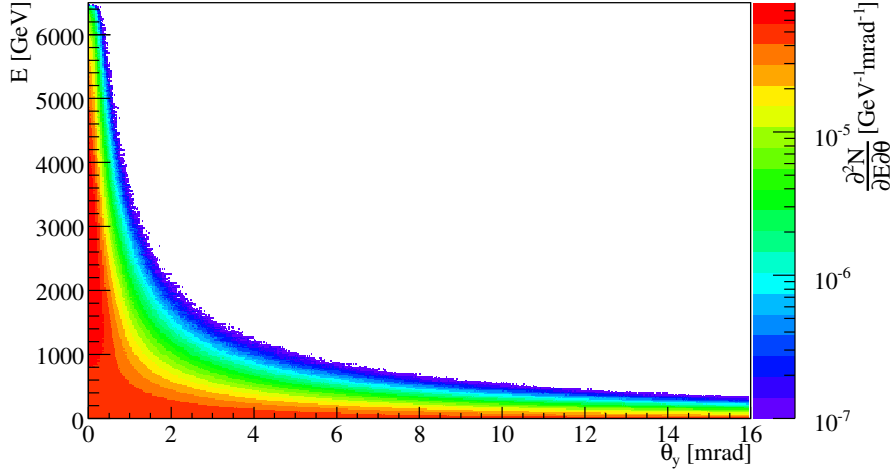


Fig. 9: Distribution of  $\Lambda_c$  for 6.5 TeV protons on target as a function of the vertical angle  $\theta_y$ , obtained using PYTHIA8.240.

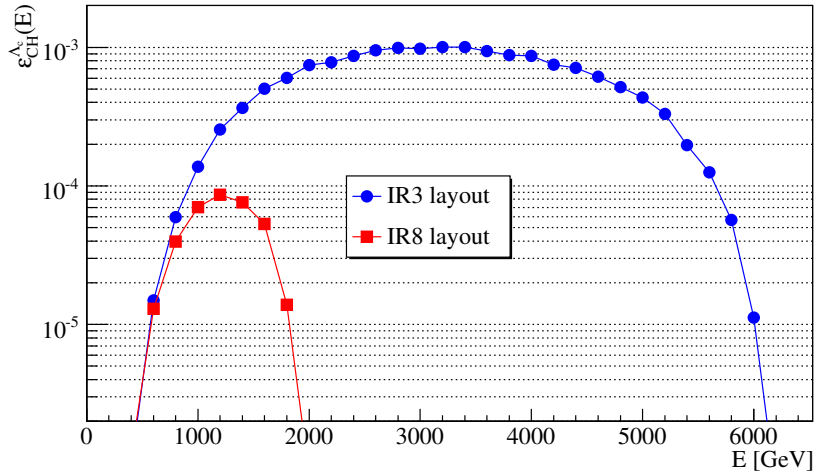


Fig. 10: Channeling efficiency of  $\Lambda_c$  channeled by the  $Cry_2$  as defined in Eq. (3).

A further step toward the evaluation of the achievable  $\Lambda_c$  yield is the convolution with the expected number of PoT and the production in the target. The number of  $\Lambda_c$  produced per impacting proton,  $N_{\Lambda_c}$ , can be calculated as:

$$N_{\Lambda_c} = N_A \rho l_t \sigma(\Lambda_c) = 0.6 \times 10^{-4} \Lambda_c / p, \quad (4)$$

where  $N_A$ ,  $\rho$ ,  $l_t$  and  $\sigma(\Lambda_c)$  are the Avogadro's number, target density, target length and total cross section, respectively. In particular  $\sigma(\Lambda_c) = 10.13 \mu b$  was used for 6.5 TeV impacting protons, as calculated using PYTHIA8.240. Note that the  $\Lambda_c$  production and decay in the target volume must be taken into account as:

$$P_t(E) = \frac{1}{l_t} \int_0^{l_t} \exp(-l/c\gamma\tau_{\Lambda_c}) dl. \quad (5)$$

The production spectrum of  $\Lambda_c$  ( $S_{\Lambda_c}(E)$ ) must be also taken into account and it is shown in Fig. 11.

In conclusion, the yield of  $\Lambda_c$  emerging from the  $Cry_2$  that have acquired the desired precession



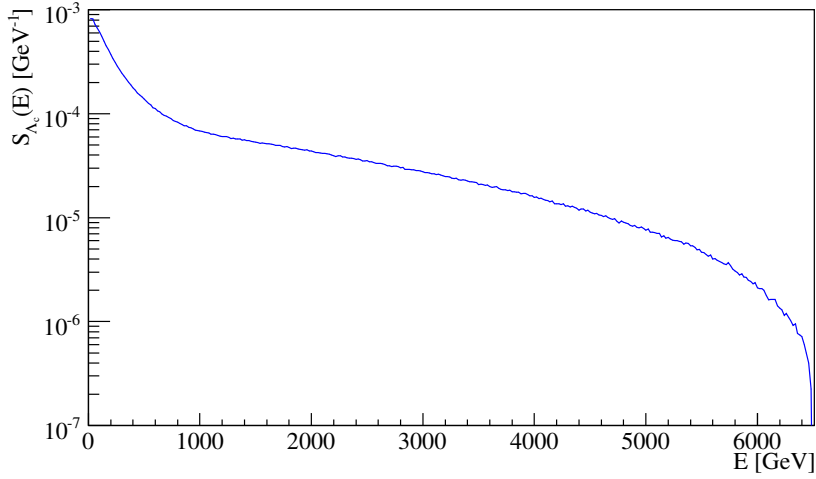


Fig. 11: Production spectrum of  $\Lambda_c$  produced by 6.5 TeV protons on target, produced with PYTHIA8.240

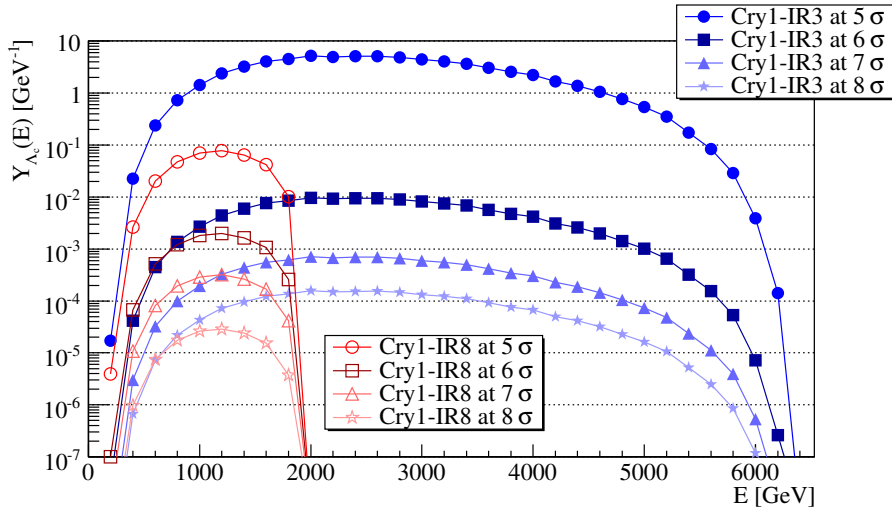


Fig. 12: Expected yield of  $\Lambda_c$  emerging from the  $\text{Cry}_2$  that acquired the desired precession in 10 h LHC fill as defined in Eq. (6). Comparisons with respect to performance of an alternative layout place in IR3 (Section 2.6) are also shown. Results are based on inputs produced with PYTHIA8.240.

can be expressed as:

$$Y_{\Lambda_c}(E) = N_{\Lambda_c} P_t(E) S_{\Lambda_c}(E) \varepsilon_{\text{CH}}^{\Lambda_c}(E) \int_{10\text{h}} P_oT(t) dt . \quad (6)$$

The  $Y_{\Lambda_c}(E)$  for the layout proposed and possible operational scenario are shown in Fig. 12, using  $\int_{10\text{h}} P_oT(t) dt$  reported in Table 4. For comparison, the expected  $Y_{\Lambda_c}(E)$  with an alternative dedicated layout, which is introduced and discussed in Section 2.6, is also reported in Fig. 12.

### 2.2.5 Possible improvements

Although a final assessment requires a careful evaluation by the experiments, it is clear that the number of protons on target achievable with a completely passive and parasitic operation of the double-crystal experiment is limited. Ways to improve the PoT and the  $\Lambda_c$  yield are discussed here as an input for possible future studies.

As shown already in the previous section, an obvious way to increase loss rates is to approach more the  $\text{Cry}_1$  to the primary beam. A rate of  $PoT \sim 10^6$  p/s might be obtained with the  $\text{Cry}_1$  at  $5.5 \sigma$ . Although the feasibility of this setup has to be demonstrated, a preliminary assessment indicates that this might provide still sufficient margins to various errors, to ensure that the hierarchy is not broken and the crystal remains a secondary collimator.

A proposal to increase in a controlled way the beam losses at the LHC is to selectively excite a portion of the beam with the transverse damper, in a similar way as it is used to perform collimation loss maps and quench tests (see for example Ref. [46]). Transverse noise can be added to specific bunches or trains, on either plane, which induces controlled losses through an emittance blow-up of the given bunches. This could be used to produce a larger flux of particles impinging on the primary collimators and thus on the  $\text{Cry}_1$ , ultimately increasing the  $PoT(t)$  function introduced above. For example, exciting 288 bunches (one batch) out of the 2555 in typical stores of 2018, achieving a beam lifetime of, say, 20 h on these bunches only, would allow to get a  $PoT \sim 10^6$  p/s with  $\text{Cry}_1$  at  $6 \sigma$ . However, the emittance blow up caused by the excitation also induces a reduction of luminosity. Thus, a compromise between the acceptable loss of luminosity and required increase of  $PoT(t)$  would need to be found. A first estimation of loss in peak luminosity as a function of emittance growth and number of excited bunches in one beam and one plane is shown in Fig. 13. This estimate is made assuming a constant bunch intensity to assess the contribution of emittance only. Further studies are needed to evaluate the expected emittance growth as a function of the desired lifetime.

Increasing the target thickness and using germanium for the second crystal can lead to a larger production of  $\Lambda_c$  and improved channeling efficiency, respectively, but both aspects would need to be studied more systematically (see for example Ref. [47]). Local losses induced by the 5 mm long tungsten target considered in this paper are acceptable for the machine with the considered settings of the first crystal, but the effect of thicker targets needs to be addressed. Possible impact on the LHCb backgrounds should also be quantified.

The single-pass channeling efficiency might be increased by up to about 10% using Ge with respect to Si [48, 49], but a solid experimental verification for the crystal parameters being considered should be pursued. The possible improvements from the usage of Ge crystals should be studied further.

A factor 2 in bunch intensity is expected in the HL-LHC era beyond Run 3, which is directly translated in a factor 2 larger PoT rates with respect to what considered in previous sections for the same loss assumptions. In Run 3, the LIU beams are expected to deliver operational beams up to 60 % more intense than in Run 2. The achievable lifetime in standard operation for these two scenarios is very hard to predict because of the difficult scaling with the bunch current and with the optics that will be deployed.

Looking further in time beyond Run 3, additional constraints can come from failure scenarios in HL-LHC. For example, crab-cavities failures can induce large bunch oscillations/rotations [50]. Thus, a significant fraction of mis-kicked bunches can be intercepted and potentially channeled by the  $\text{Cry}_1$ . Hence, a safety margin with respect to TCPs must be computed, which can be larger than the  $0.5 \sigma$  considered above (TCPs are at  $5 \sigma$ ). On the other hand, hollow electron lens (HEL) may be installed in HL-LHC [51], which will be used for an active control of beam tails. The presence of HEL will mitigate losses on the primary aperture during failure scenarios, possibly allowing for similar safety margin of  $0.5 \sigma$ , and could even be provide the possibility to have more freedom to act on halo particle. Nevertheless, these options should be studied in detail and the impact on the expected performance due to the reduced population and increased diffusion speed of the beam halo that is generated by the HEL must be evaluated.

Constraints can come also from possible damages to the detectors. The LHC collimation system is designed to withstand the failure scenario of beam lifetime drops down 0.2 h for 10 s. With LHC operational settings in 2018,  $\text{Cry}_1$  at  $5.5 \sigma$  and 200 h of beam lifetime an average  $PoT$  rate of about  $10^6$  p/s is expected. Thus, a lifetime of 0.2 h will directly translates in PoT rates of about  $10^9$  p/s. A beam dump request is triggered by LHCb if dangerous events rate are approached. Thus, no damages should

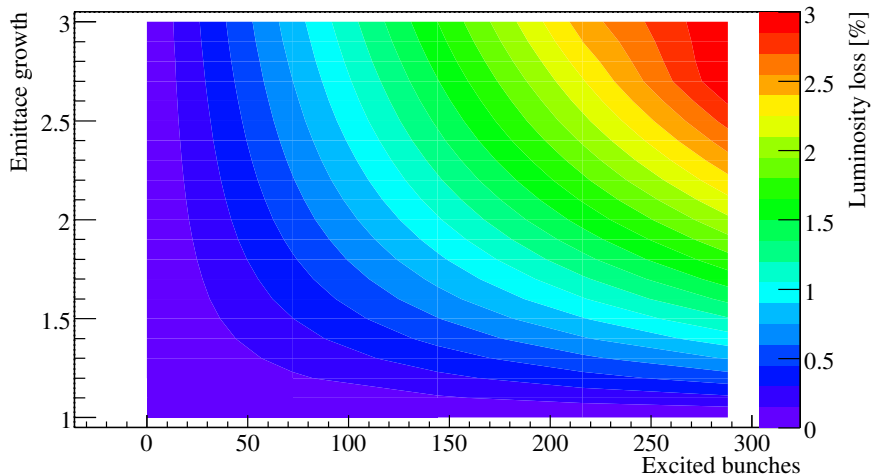


Fig. 13: Loss in peak luminosity as a function of emittance growth and number of excited bunches in one beam and one plane.

be caused but energy simulations are needed to assess this limit in LHCb, to set appropriate margins on sustainable PoT rate during operations and failure scenarios. However, LHCb should not affect the machine availability in this scenario (see also below).

### 2.3 State-of-the-art of developments for long crystals

A key requirement for assessing the feasibility of the double-crystal concept is the demonstration that crystal channeling with large bending angles, above 10 mrad, is achievable reliably and with sufficient efficiency at the energies of interest. The first observation of  $\Sigma^+$  magnetic moment precession in bent crystals [26] was obtained with crystals providing a bending of 3.7 mrad. The IR8 implementation requires a factor 4 more bending at significantly higher  $\Lambda_c$  energies. Experimental studies carried out at CERN in the 90's (see for example Ref. [52]) demonstrated channeling at larger angles, up to about 11 mrad, with efficiencies of about 2 % for 450 GeV proton beams at the CERN SPS. Earlier measurements with promising results are reported in Ref. [53], showing 16 % efficiency for a 8.5 mrad bending. The extrapolations to the crystal parameters needed for the IR8 double-crystal setup are not straightforward. This was identified as a critical item to be followed up in the PBC fixed-target working group.

An R&D program was launched to experimentally validate this type of crystals with hadron beams at the highest available energy. This effort was started by the UA9 collaboration, using proton, pion and ions beam in the SPS-H8 extraction line, with energies up to 400 GeV, and was followed by another initiative (in the context of the SELDOM (Search for the electric dipole moment of strange and charm baryons at LHC) research program, using LHCb H8 infrastructure). Important results were obtained very recently, in measurements carried out at the end of the 2018 run, with pion beams at 180 GeV. The preliminary results are very promising, though still unpublished at the moment of writing. A preliminary analysis was presented to the PBC fixed-target working group. Measurements from both teams indicate that channeling efficiencies above 10 % were achieved with the latest crystal technology, and for bending parameters close to the ones that are being proposed for the IR8 implementation. The results achieved so far are encouraging and demonstrate the feasibility of the long-bent crystals. The scaling of the channeling efficiency with the beam energy can be predicted by simulations, though, until measured in the LHC, remains a possible source of uncertainty.

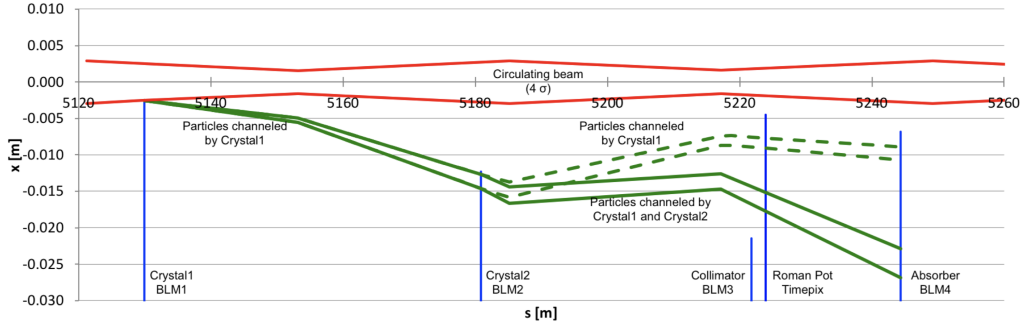


Fig. 14: Horizontal beam envelope (red) and of the double-channeled beam (green), with the single-channeled beam shown by the dashed lines, and position of the main devices in the UA9 Experiment installation (blue lines): beam loss monitors (BLM), Roman pot and absorber. All devices are in the horizontal plane [29].

### 2.4 Feedback from first double-channeling observations at the SPS

An experimental apparatus to test the double-crystal scheme in the SPS was set up by the UA9 collaboration and was operated in 2017 and 2018. It is illustrated in Fig. 14, from Ref. [29]. The goal of the data taking runs in 2017 was to demonstrate the feasibility of the double-channeled process, to define the operational procedures for future measurements and to assess the possibility to measure the efficiency of the double-channeling process with existing or upgraded detectors.

The first operation to perform in order to obtain the double-channeled beam – i.e. to channel a second time the halo that emerges from  $Cry_1$  – is the alignment of  $Cry_1$ . This follows the well-established procedure based on observation of local losses in dedicated beam loss monitors (BLMs) that reach a minimum in the optimum channeling orientation. One BLM is available downstream of each movable device, including the absorber. A similar procedure was applied with the second crystal. Its position was adjusted until it was placed in the path of the deflect halo and its angular orientation then varied. In this setup, local losses cannot be used to align the  $Cry_2$ , because the reduction of losses due to channeling is hidden by the high level of losses from upstream devices. Beam loss monitors at the absorbers (see “BLM4” in Fig. 14) were used to detect when the double-channeling was established, through a linear scan that revealed the presence of both beamlets. An image of both beamlets, recorded with a medipix detector located between  $Cry_2$  and the absorber, is shown in Fig. 15. This is an important result towards the feasibility demonstration of the double-crystal concept.

These first results, further extended in 2018 by adding a real target upstream of the second crystal [28], are promising and have illustrated that from the machine side, the setup of the experimental apparatus is feasible. Further studies should be focused on the feasibility of channeling the particles of interest produced by the interaction of the channeled beam with the target, and on the demonstration that they can be separated by the second crystal from the main proton beam that is scattered on the target.

The SPS setup provides an ideal environment for such detailed studies and is seen as an extremely useful playground prior to, or in parallel to, a possible deployment at the LHC.

### 2.5 Relevant LHC machine aspects

#### 2.5.1 Introduction

In this section, we discuss aspects related to the impact on the LHC from a possible installation of the double-crystal setup, in addition to the aspects related to the integration into the collimation system and to the machine protection, discussed above.

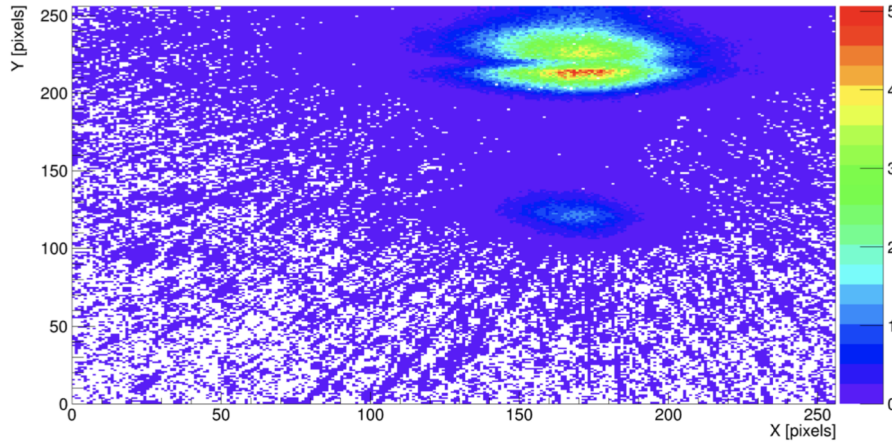


Fig. 15: Image of the single-channeled (top) and double-channeled (middle) beams on the Timepix detector (see Fig. 14, at the position of about 5225 m). The image should be rotated by  $90^\circ$  counter-clockwise in order to reproduce the real spatial position of the beams. The color scale represents the average number of counts per second per pixel [29].

The following items have been identified:

- collimation and machine protection;
- machine aperture compatibility;
- controls and beam interlocks compatibility;
- impact on machine impedance;
- impact on electron cloud;
- impact on operational efficiency and commissioning;
- background induced in the experiments.

At this stage, these can only be seen as preliminary considerations and guideline for future work, because the design of the new devices does not exist. When applicable, the present design of the crystal assemblies for beam collimation is considered as reference. It is briefly recalled in the following.

The new devices for the double-crystal experiment are particularly challenging because, for the IP8 scenarios, they must be installed in areas of the accelerator where the beams share a common beam pipe, which adds additional constraints in terms of aperture, impedance and electron cloud.

The crystals for beam collimation studies installed in IR7 are designed with a specific “O” shaped replacement chamber, of the same diameter of adjacent vacuum chambers, as shown in Fig. 16, taken from Ref. [30]. This replacement chamber is preventing to move the crystals in the beam in phases when they are not needed. It is moved out (i.e., shifted downwards for the configuration in Fig. 16), allowing crystal movement into the beams, when needed. In this case, an horizontal crystal is considered. A similar design could be considered for the fixed-target experiment devices. The replacement chamber would have to moved out, allowing crystal/target insertions, for all phases of the operational cycle, for the fills when data taking are planned. Another alternative is to optimize further the design, making it compatible to high intensities (see sections below) without need for a replacement chamber.

### 2.5.2 Aperture constraints and considerations on controls aspects

Crystal and target devices are movable objects that will be set at the operational positions only when needed for data taking and retracted in “out” positions in all other phases of the LHC operational cycle, in a similar way as the VELO or the Roman pots are operated. Clearly, non-movable parts must be

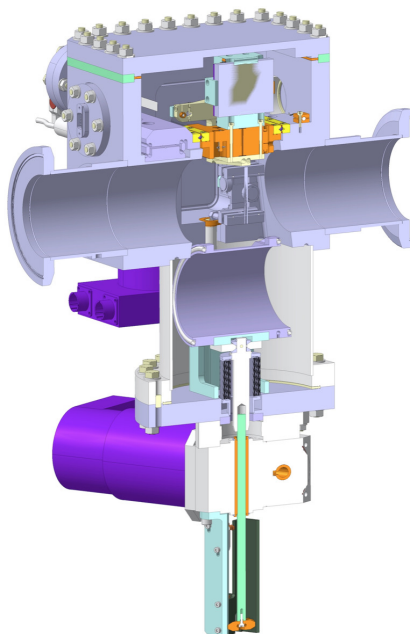


Fig. 16: Design of the crystals for beam collimation installed in IR7. The graph shows a horizontal crystal. A in-vacuum, round replacement chamber is inserted in the beam when the crystal is not used, providing a full compatibility with the high-intensity beams. It is moved vertically out of the beam, as shown here, to enable inserting the crystal in the beam.

designed to respect local aperture constraints and not to add aperture restrictions. The control system must respect the standards in terms of accuracy and interlocking aspects that are applied to other LHC movable devices capable to approach the beam [31]. A simplification with respect to the collimators and crystals for cleaning is that experimental devices are not required to move through functions of time, as they are used only in stable beam conditions for physics data taking.

An optimized position interlocking strategy must be defined, as done for example for present crystals IR7 and for the Roman pots that have been used in IR1/5 since Run 1. This involves specific position interlock thresholds defined by operation/collimation teams to ensure the compatibility with the LHC aperture constraints and to ensure that beams are safely dumped if the devices are accidentally moved too close to the circulating beams.

More specific aspects of the aperture compatibility of crystals and targets in their “in” beam positions are addressed in the collimation section above that describe a possible integration into the transverse hierarchy of the multi-stage cleaning system. Clearly, specific settings will have to be defined for the Run 3 configuration.

It is also noted that the LHCb experiment is operated at levelled luminosity, achieved by reducing as a function of time the vertical beam-beam separation. All the components of the proposed layout are also in the vertical plane, and are longitudinally located within the separation bump. Thus, dynamic changes of settings may be needed during the physics data taking, to follow closed orbit movements. Otherwise, at every step the beam will be moved further apart from the first crystal (the separation bump is reduced and the beams approached to the center of the beam pipe.).

### 2.5.3 Impedance

The impedance of crystal devices is a serious concern that demands an optimized design for all the components that needs to be inserted during high intensity operation at the LHC, in particular for proton beams. The crystal devices used for collimation studies in IR7 have been studied to assess their com-



patibility to high-intensity operations. The solution based on the replacement chamber, described in the previous section, ensured a safe operation of IR7 crystals in the Run 2 proton run. It is being studied if the present goniometer is compatible with the high intensity proton beams foreseen for Run 3 and Run 4. Clearly, a scenario where the goniometer must be compatible to high intensities, applies to the new devices for the double-crystal setup because, in the parasitic operational mode, they need to be exposed to high proton beam intensities for the fills for data taking.

Studies are ongoing to make the crystal assemblies for collimation compatible to high intensities [32]. The outcome of this work to optimize the design could be applied also to the fixed-target devices. Note however that a significant difference with respect to IR7 goniometers is that both beams will see the goniometers in IR8 (one installed between D1 and D2, and one just upstream IP8 in the beam 1 direction). It is likely that the design of the crystal/goniometer assembly must be optimized further, and most likely need to include a dedicated cooling system.

The contribution to the total machine impedance budget due to presence of additional collimators around the ring, also needs to be studied.

#### 2.5.4 *Vacuum*

Any device exposed to the LHC beams must respect the strict vacuum constraints described in Ref. [33], in particular the movable devices that can move close to the beam. Constraints for bake out are particularly demanding for high-precision movable devices. The present LHC crystal collimator design is fully compatible with the vacuum requirements and uses components that are compatible with the standard bake-out temperature of 250 C adopted at the LHC. We consider therefore that no issues are expected from the vacuum point of view, although clearly the final design shall be elaborated with vacuum constraints in mind. This includes a careful choice of material and qualified procedures for their machining.

#### 2.5.5 *Potential impacts on operational efficiency*

Devices for fixed-target experiments shall be treated as Roman pots that are operated under the shared responsibility of the LHC operation and collimation teams and comply to the standard controls implementation for a safe operation of movable devices. This includes the connection to the beam interlock system. The hardware commissioning of all components and the verification without beam on the interlocking system would be under the responsibility of the experiment team.

The beam commissioning of these devices must also follow the standard procedures for settings validation through loss maps and intensity ramp-up. A detailed description of these procedures, applied at the beginning of each operational year and several times throughout the year upon changes of configurations, goes beyond the scope of this document. It is however important to note that these operational and machine protection constraints must be systematically fulfilled prior to even individual insertions at high intensities.

Typically, this involves (1) a setup early on in the operational year, e.g. as soon as the collimator's final settings are put in place; (2) inclusion of setting management of fixed-target devices into the operational sequences used to drive the LHC; (3) validation through loss maps and asynchronous dump tests in all relevant machine operational phases; (4) validation of operational configurations during the intensity ramp up that, in every operational year, precedes the operation at maximum beam current. In this context, it is important to define as soon as possible the operational scenario for fixed-target experiments, i.e. if a parasitic or dedicated operational mode should be expected. This will enable preparing the specific procedures and assess the detailed impact on the initial setup and commissioning for proton operation.

### 2.5.6 *Electron cloud*

No problems with the present LHC design are encountered. Nevertheless, the IR7 goniometer was never exposed to high-intensity 25 ns beams so we lack still an experimental demonstration (this could perhaps be planned in Run 3 if necessary). Further studies are needed to avoid local heating due to e-cloud. The material choice for target and new components must be optimized, taking e-cloud build-up into account, for all future devices.

### 2.5.7 *Background to experiments*

The simulations described above indicate that losses on tertiary collimators around the ring are not significantly affected. These are the main sources of halo-induced background, which are typically small at the LHC [34]. The assessment of local losses in LHCb should be assessed under the responsibility of the LHCb collaboration.

It is important to note that LHCb shall study the failure scenario with peak losses on the primary collimators of about 500 kW (LHC) and 1000 kW (HL-LHC), corresponding to the case when peak losses occur at maximum beam intensity, when the crystal apparatus is put in place. The design criterion shall be that the detector must survive without dumping the beam at the occurrence of these peak loss rates, for consistency with what applies for other critical loss locations.

## 2.6 **Alternative layouts under studies: a new layout for the LHC IR3**

The main motivation to look for another possible layout comes from the need to overcome intrinsic limitations that are present in IR8 that were identified as:

- Large required bending of the Cry<sub>2</sub> to respect the acceptance of LHCb;
- Limited possibility to mitigate beam losses because of the combination of optics at the crystal and at the collimators, which limits the betatron cut achievable with this setup.

This motivated the study of alternative locations in the LHC to carry out a similar experiment. Our choice was to study IR3: it is a warm insertion where collimators are already available and there is significant longitudinal space available. In this region where the beams are separated, one could even think to house two independent experiments.

The design of a double-crystal layout in IR3 is shown in Fig. 17. The optimization is described in Ref. [20]. The Cry<sub>1</sub> with bending  $\theta_b^{\text{Cry}_1} = 50 \mu\text{rad}$  and length  $l^{\text{Cry}_1} = 4 \text{ mm}$  is installed upstream of the dogleg dipoles (gray boxes). The reduced constraints on longitudinal space available and the smaller  $\beta(s)$  function with respect to IR8, made it possible to improve the performance of the additional collimators that are also needed in this case. Four are added as in IR8, with the same assumptions for the materials. Using the same TCSGs settings of  $10 \sigma$  the angular cut performed is of about  $20 \mu\text{rad}$  (i.e.  $\times 3$  smaller than in IR8). The bending of the second crystal can be significantly reduced, increasing the yield of channeled  $\Lambda_c$  that acquired the desired precession. The target is still 5 mm long and made of tungsten, for a direct comparison to the IR8 case. The drift space between the Cry<sub>2</sub> and the next downstream magnet is about 70 m, leaving room for a dedicated experimental apparatus yet to be designed. The main layout parameters are reported in Table 5.

Another important difference with respect to the IR8 layout is that the magnets in this insertion are warm, as opposed to the superconducting magnets in IR8. Thus, reduced constraints on sustainable beam loss and relative magnet lifetime are present in IR3.

A clock-wise orientation (apparatus installed on beam 1) of the layout is adopted because possible debris from the absorbers goes to IR4 (where the RF is placed) rather than to IR2 (where the ALICE experiment is located).

An notable advantage of IR3 is that the two beams are in two separated vacuum pipes and do not interfere with each other. Thus, it could be considered to have a mirror layout in Beam 2 that shares a



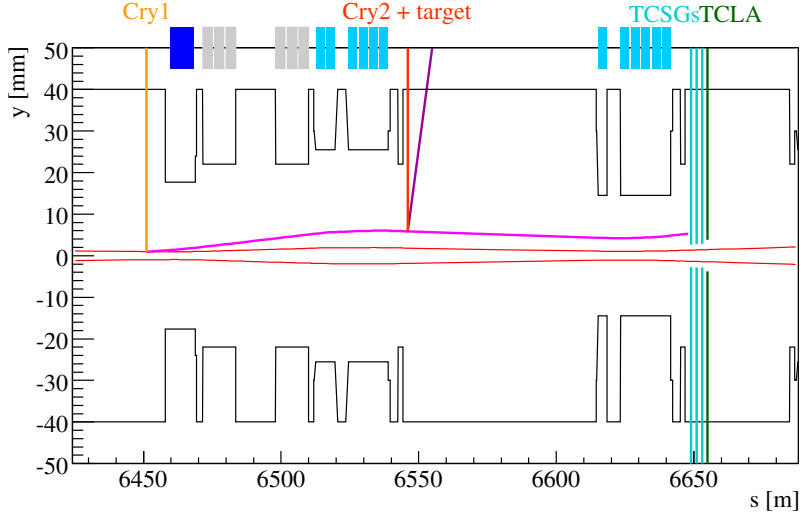


Fig. 17: Layout of a double-crystal experiment in IR3, following the same notation as in Fig. 2. Warm quadrupoles and dipoles are shown by the light blue and gray boxes, respectively.

Table 5: Installation position and main features of the proposed experimental layout in IR3. All the components act on the vertical plane.

Name	$s$ from IP1 [m]	Bending [ $\mu$ rad]	Length [cm]	Mat.	Bending planes
Cry <sub>1</sub>	6451	50	0.4	Si	110
Target	6546	-	0.5	W	-
Cry <sub>2</sub>	6546	5000	7.5	Si	110
TCSG.A4R8.B1	6649	-	100	CFC	-
TCSG.B4R8.B1	6651	-	100	CFC	-
TCSG.C4R8.B1	6653	-	100	CFC	-
TCLA.A4R8.B1	6655	-	100	W	-

common detector in the 70 m drift space. This will require duplicating the hardware of crystals, target and absorbers but can open the possibility to either perform different studies in the two beams<sup>4</sup> or double the statistics. This possibility clearly needs more studies.

The beam loss pattern obtained with the Cry<sub>1</sub> at  $5\sigma$  (i.e. same aperture of the TCP) is shown in Fig. 18. The aperture of TCSGs and TCLA in IR3 is  $10\sigma$  and  $13\sigma$ , respectively, in order not to interfere with the multi-turn betatron cleaning process. In principle this layout would allow *parasitic* operations during standard LHC operations also with such a tight Cry<sub>1</sub> setting. The loss pattern in Fig. 18 does not show any peak of cold losses above the threshold defined by Fig. 5. This is mainly due to the reduced bending and length needed for the Cry<sub>1</sub> and the tighter angular cut performed by the TCSGs in IR3, with respect to the IR8 layout. Thus, less protons experience nuclear interactions in the Cry<sub>1</sub> itself and are intercepted by the TCSGs more efficiently. Simulations with different Cry<sub>1</sub> aperture were carried out and the achievable instantaneous and integrated PoT during one fill were produced as done for IR8 (see Fig. 8). A summary of what can be achieved is reported in Table 6. Contrary to the case of IR8 (see Table 4), a parasitic running scenario with Cry<sub>1</sub> at  $5\sigma$  is in theory possible from the point of view of cold losses. Other aspects such as machine protection implications need to be assessed. See Ref. [3] for more details.

<sup>4</sup>e.g. target+Cry<sub>2</sub> assembly optimized for dipole-moment measurement of different particles.

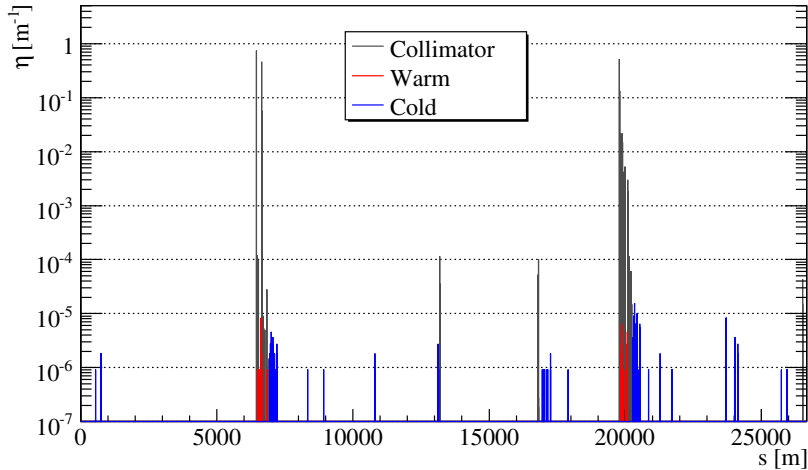


Fig. 18: Simulated beam loss pattern for the IR3 layout with  $\text{Cry}_1$  at  $5\sigma$ . ( $1\text{ p} = 9.1 \times 10^{-7}\text{ m}^{-1}$ )

Table 6: Fraction of simulated protons that hit the  $\text{Cry}_1$  in IR3 and relative channeling efficiency, together with the assumed number of bunches,  $N_b$ , and the integrated proton flux in a 10 h fill with 200 h beam lifetime. Note that, contrary to the case of IR8 (Table 4), a parasitic running scenario with  $\text{Cry}_1$  at  $5\sigma$  is in theory possible from the point of view of cold losses. Other aspects such as machine protection implications need to be assessed.

$\text{Cry}_1$ setting [ $\sigma$ ]	$N_b$	$\frac{N_{\text{imp}}^{\text{Cry}_1}}{N_{\text{sim}}}$	$\varepsilon_{\text{CH}}^{\text{Cry}_1}$	$\int_{10\text{h}} PoT(t)dt$ [p]
5	2556	0.78	0.66	$2.8 \times 10^{12}$
6	2556	$2.4 \times 10^{-3}$	0.40	$5.2 \times 10^9$
7	2556	$2.7 \times 10^{-4}$	0.26	$3.8 \times 10^8$
8	2556	$1.3 \times 10^{-4}$	0.12	$8.4 \times 10^7$

### 3 Internal solid target and single-crystal implementation

As discussed in Refs. [10, 11], fixed-target experiments that make use of the LHC proton and lead beams allow one to probe the hadronic matter in uncharted kinematic domains as well as the quark gluon plasma and can provide crucial inputs to cosmic ray physics. An internal solid target installed in the LHC beam pipe can either use the beam halo or the beam channeled by a crystal installed prior of the experiment. In both cases, it is valuable to use various target materials from low to large atomic mass numbers to access a rich physics programme. From the LHC machine and host experiment, the following aspects need to be studied:

- impact on collimation and machine protection,
- impact on machine impedance,
- impact on machine vacuum,
- compatibility of each target species with the LHC conditions,
- controls and beam interlock compatibility,
- background induced on the host experiment.

In the following, the option of the solid target on beam halo will be briefly discussed. A fixed-target scenario that makes use of the ALICE experimental device in the LHC by using a bent crystal as proposed in Ref. [12] will be described in more details.

### 3.1 Solid target on beam halo

Conventional solid target setups where the beam halo directly interacts with the in-vacuum target, as shown in Fig. 1 (panel b), have been envisioned by the working group. As in past and current experiments [15, 18], wire or foil targets of the order of  $500 \mu\text{m}$  thickness could be considered. The solid target can degrade the beam vacuum and impact the beam impedance. A retractable target system is required to cope with the main beam envelopes at beam injection. A linear movement with high precision is needed in order to set the distance of the target to the beam halo and to follow any new optics of the LHC beams during the years. Although members of the ALICE collaboration expressed interest in these possible scenarios [54, 55], detailed layouts for these setups have not been studied and presented in the working group and this option will not be discussed further in this document.

### 3.2 Crystal beam splitting on solid target in IP2

The double-crystal setup Fig. 1 (panel a) can also be used in a single-crystal setup where the deflected halo interacts with a solid target internal to the beam pipe close to an existing detector. In that case, similar machine studies as in the double-crystal setup discussed in Section 2 need to be carried out.

A specific implementation of the single-crystal setup was proposed for an experiment in IP2 with the ALICE detectors [12]. A possible layout for this proposal is shown in Fig. 19. A small bent crystal,

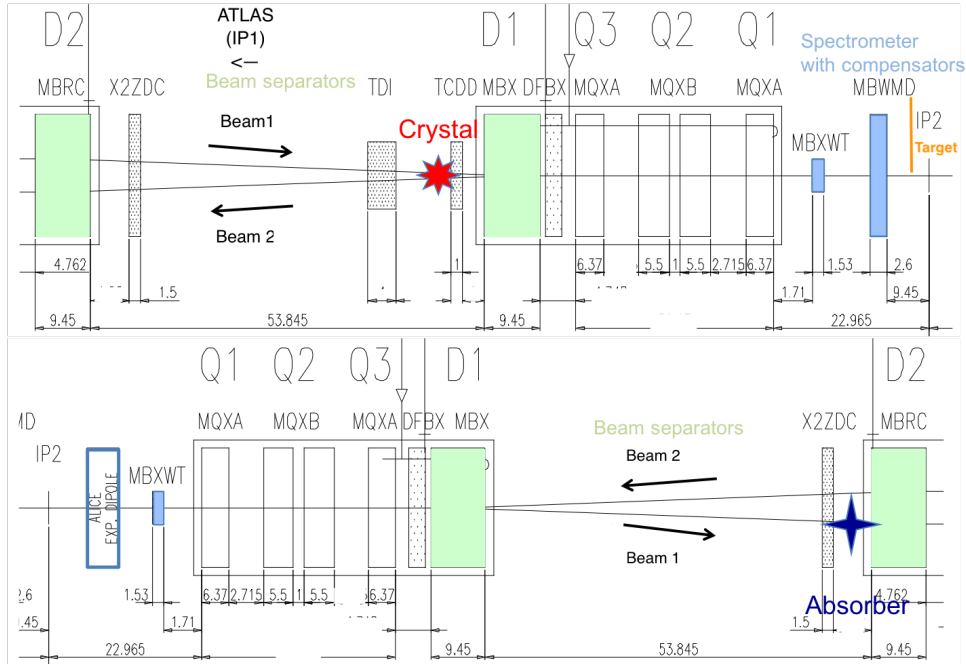


Fig. 19: A possible layout for an internal fixed-target experiment at IP2: a bent crystal is used to deflect the beam halo onto an internal solid target located near IP2. An absorber is located downstream.

of the size of few millimetres and mounted on an appropriate goniometer [56], could be located upstream of the focusing triplet, just before the TCDD absorber, to channel and deflect the halo particles of LHC beam 1 horizontally, as shown in Fig. 20. The target could be located in one of the positions marked in orange in Fig. 20. A deflection of the beam halo by  $250 \mu\text{rad}$ , 72 m upstream the Interaction Point 2 (IP2), would allow one to place the target at a safe distance of 8 mm from the beam center. The non-interacting particles could be disposed of in an absorber located between the Zero-Degree-Calorimeter (ZDC) and the focusing triplet. The deflected particles follow the green trajectory in Fig. 20. The interacting beam halo particles will produce particles into the ALICE detectors, whilst the non-interacting particles will continue their path up to the absorber where they should be adequately collimated. In a more detailed study, the exact number of collimators needed for this purpose should be defined.

### 3. Internal solid target and single-crystal implementation

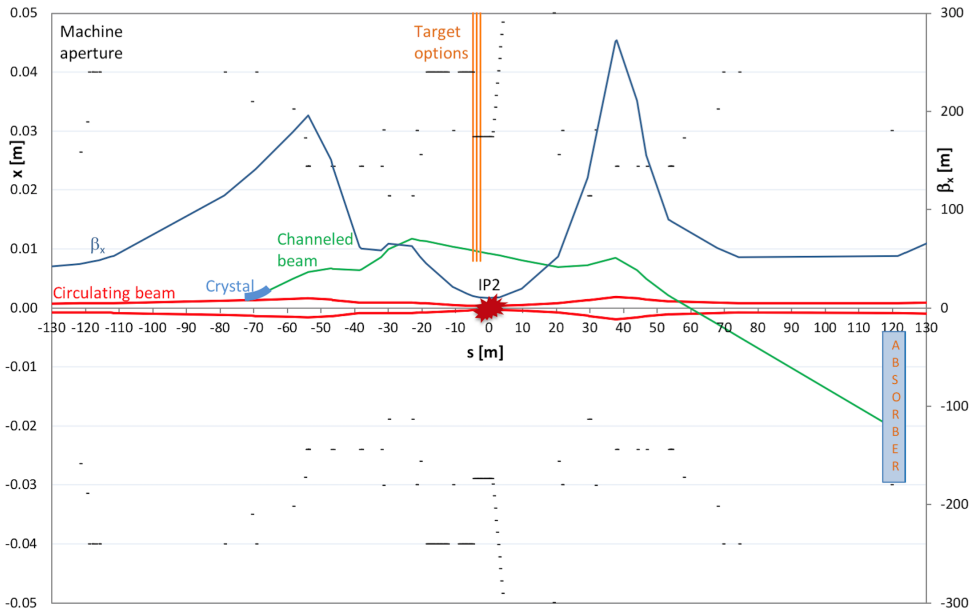


Fig. 20: Particle trajectories for an internal fixed-target experiment: a bent crystal splits and deflects the halo (green) from the circulating beam (red), and sends it on an internal target (orange) placed in front of the ALICE detectors; the non-interacting channeled particles are caught by an absorber downstream; a safe distance is maintained between the channeled beam (green) and the machine aperture (black).

As in the case of the studies performed for IP8 in Section 2.2, detailed studies are needed to assess the feasibility of this layout and the flux of protons on target ( $PoT$ ). In IP8, a vertical deflection of the beam halo is preferred and this scenario could be also envisioned in the case of IP2. At a first approximation, a similar order of magnitude for the proton flux as in IP8 is expected, i.e. with a rate of at least  $\sim 10^6 PoT/s$  that could be increased with further studies to  $\sim 10^7 PoT/s$ . The formalism for the estimation of proton losses (and for their control if one needs to actively induce losses on some bunches) is identical to the IP8 formalism. The difference between IP2 and IP8 lies in the specific local distribution of the multi-turn halo.

In addition, the proposed layout aims at running with the lead beam where studies have not been carried out so far. It is important to note that, with heavy ion beams, the parasitic scheme where the crystal sits at settings of secondary or tertiary collimators, might not work. While the multi-turn halo is still composed of protons with proton beams, ion beam halo undergoes fragmentations and dissociations upon interacting with primary collimators of IR7. So, higher-order halos include ions of different species. In the parasitic scheme, the composition of the channeled ion beam should then be evaluated. A dedicated operational mode with the crystal as primary collimator would not entail this complication, but local losses and the compatibility with the standard ALICE physics programme could become potential concerns. Other issues that will be investigated in the future concern the LHC machine aspects, such as the machine protection and the compatibility of the fixed-target operation with the collimation operation, as described in Section 2.5.

#### 3.2.1 Internal solid target setup

A possible design for the internal solid retractable target is shown in Fig. 21 in the case of a one-target system. It is possible to design a setup with more than one target, allowing one to use various target types. The target system dimension is  $170 \times 50 \times 50 \text{ mm}^3$ .

Several materials are under investigation for the target with low, medium and high atomic mass

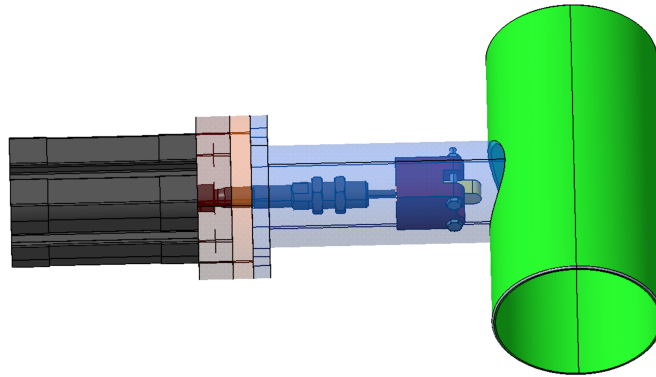


Fig. 21: Setup for an internal solid target with a one-target system. On the right side the pipe section is shown in green. Leftwards are visible the target (yellow), the target holder (brown), the actuator (black) and flanges (pink and orange) with a gasket inside. In translucent blue is the tapping of the pipe.

number. Other constraints shall guide the material for the target itself as well as for the target holder and any other piece close to the interaction between the deflected halo and the target. Among the tight constraints are the compatibility with the vacuum and the melting point of the target material that should be large enough to cope with the channeled LHC beam, in particular with the proton beam. The excess heat must be drained off the target and its holder, in designing dedicated geometry. Light materials could be Be, Ca or C. For heavy materials, Os, Ir or W are good candidates. Middle mass materials such as Ti, Ni or Cu could be used. Each target shall be manufactured in an oblong shape, with a radius of 2.5 mm and a total length of approximately 17 mm. The efficient part of the target is the final round shape, with a thickness that may vary from 0.2 to 5 mm depending on the achievable particle beam flux and the detector rate capability.

The target holder is designed for maintaining the target between its two sides like a press. This contact holding provides the advantage of a sufficient surface between the target and the holder for heat removal.

The top of the holder is connected to the rod of the actuator. Located in a new dedicated tapping, each actuator must be a single-effect pneumatic actuator with two positions: a parking position out of the pipe and a nominal position inside the pipe activated by pressurised air. An electro-valve distributor controls the position of each actuator through a plastic hose and is away of the setup. This is helpful to reduce shadow to existing detectors. When the distributor stops delivering pressure, a spring inside the actuator puts the rod (and so the holder and the target) back in the parking position. This design provides also a safety position in case of power breakdown. The interface between the inner part of the pipe (vacuum) and the outer environment needs a fine study (mechanical feedthrough). Each tapping receives the target, its holder and the moving parts of the actuator (rod and shock absorber). The static part of the actuator (body) is out of the vacuum.

Such target system could be integrated in front of the ALICE solenoidal magnet at approximately 5 m from the interaction point in front of the existing valve that will be located at 4.8 m from IP2 in Run 3. The target can outgas and the beam pipe section around the target system has to be isolated by adding a new valve, possibly at 8.3 m from IP2, in order to maintain a high vacuum level in IP2.

Other issues that need to be investigated, in parallel to the target optimization and to the crystal implementation, is the impact of the setup on the beam impedance (for a general discussion, see Section 4.5), machine protection and machine collimation. The crystal and target devices could be installed in IP2 during LS3 but not before given the studies needed from the machine and experimental sides and the installation of a new valve.

## 4 Gaseous targets

A rich fixed-target physics programme [57, 58] has been initiated in LHCb, at LHC interaction point 8 (IP8), by exploiting the forward geometry of the detector and the availability of SMOG [59], a gas injection system originally implemented for measuring by beam-gas imaging the luminosity of the colliding beams [60]. This triggered new proposals for internal gas targets at the LHC, with or without polarisation [10–13, 61]. The list of *unpolarised* gaseous target types that are being considered includes the noble gases He, Ne, Ar, Kr and Xe and the gases H<sub>2</sub>, D<sub>2</sub>, N<sub>2</sub> and O<sub>2</sub>. The considered *polarised* gas targets are atomic hydrogen (H), atomic deuterium (D) and the helium isotope <sup>3</sup>He. Typical areal densities assumed in these gas target proposals range from a few times 10<sup>12</sup> to a few times 10<sup>14</sup> nuclei/cm<sup>2</sup>, depending on the gas type and physics addressed.

In Fig. 1 (panels c and d) the unpolarised and polarised gaseous targets in front of a forward spectrometer are sketched. One salient feature of these proposals is the use of a storage cell, further described below. The storage cell is a cylindrical open-ended tube located around the beam, which allows one to enhance the target thickness as compared to a free atomic beam or an equivalent flux of unpolarised gas injected directly in the beam vacuum, as done with the current SMOG in LHCb.

For unpolarised gas, other options (such as a gas jet, a cluster jet, or pellets [62, 63]) were also presented in the working group. These sources of unpolarised gas may provide higher target densities and a considerably smaller interaction region than the storage cell gas target. However, they require a relatively large space for their equipment which would complicate the interface to an existing detector, such as the LHCb VELO or the ALICE detector. The storage cell method appears to be the least intrusive and most cost-effective method. In addition, target thickness limits are imposed from operational requirements of the LHC (as discussed in Section 4.2) which can already be reached with the storage cell technique. Given the strong interest to install a fixed-target setup during LS2 and given the fact that the storage cell method, despite the lower target thickness, allows one to cover a broad physics program, the WG's effort focused on this option and the others were not further considered.

For any gas target implementation, a number of aspects have to be carefully evaluated to minimize impact on the LHC experiments and on the LHC machine. Each of the following points may limit the target areal density or even prohibit its use:

- vacuum system compatibility,
- dynamic vacuum effects (mostly through surface bombardment),
- impact on beam life time and luminosity reduction in the colliding beam experiments,
- limits due to local beam losses,
- impact on equipment through radiation damage,
- wake field and impedance effects (local heating and/or beam instabilities),
- aperture limitations and machine protection,
- background induced on the host experiment and/or on experiments located at the other IPs.

Any gas target implementation in the LHC must address these points. The SMOG upgrade implementation (SMOG2), described below, is used for illustration of such implementation studies.

For the case of polarised targets, additional challenges may arise that are related to the preservation of the target nuclear polarisation.

### 4.1 Types of gases and their impact on the LHC

Crucial for the LHC operation and performance is the state of the surfaces directly exposed to the beams. Desorption or emission phenomena (collectively named dynamic effects) may be ignited by the beam presence, through the strong electromagnetic fields which accompany the particle bunches and through surface bombardment by photons, electrons and ions [64]. To mitigate such effects, most of the warm



beam pipe sections of the LHC are coated with Non-Evaporable Getter (NEG) materials, usually  $2\ \mu\text{m}$  thick and predominantly based on TiZrV alloys [65] which strongly reduce the desorption/emission yields. The gas types that are proposed as LHC targets for physics can be classified in two broad categories, according to their behaviour on NEG-coated surfaces: noble gases (He /  $^3\text{He}$ , Ne, Ar, Kr, Xe) and getterable gases<sup>5</sup> ( $\text{N}_2$ ,  $\text{O}_2$ ,  $\text{H}_2$  / H,  $\text{D}_2$  / D). ( $\text{N}_2$ ,  $\text{O}_2$ ,  $\text{H}_2$  / H,  $\text{D}_2$  / D).

Noble gases are not pumped by the NEG-coating of the warm LHC beam pipe surfaces in and around the experiments. They freely travel towards the cold sections and the main effect to be considered is a possible accumulation on a cold surface which changes the properties of that surface that are relevant for the dynamic vacuum. The desorption of condensed noble gases and gas mixtures from cryogenic surfaces has been studied [66] and shows a clear dependence on the noble gas mass, more favorable for the heavier than for the lighter ones. However, the dynamic effect at the LHC that has proved to be the most performance-limiting is the electron cloud (as a result of electron multipacting). The Secondary electron Emission Yield (SEY) for noble gases at low temperature has been measured as a function of the number of accumulated monolayers [67]. The large SEY of such gases may limit the tolerable amount of gas injected in the fixed-target experimental region. Molecular flow simulations may help to estimate more precisely the tolerable amount. A procedure for liberating the beam screen surfaces from the accumulated gas and migrating it to the cold bore has been developed and tested in the LHC, by raising the temperature in a controlled manner [68]. This method may be successfully applied for He, Ne and Ar gases condensed on the experimental side of the warm-to-cold transitions of the inner triplets in a relatively short time compatible with a typical LHC year-end technical stop. However, for Kr and Xe the temperature to be reached is too high ( $\sim 120\ \text{K}$  and  $\sim 160\ \text{K}$ ) for this procedure to be applied in such a short break. It would require an almost complete warm-up of the inner triplets. The constraints and mitigation measures to be considered for these two gases are therefore more laborious than for the lighter noble gases.

The getterable gases  $\text{N}_2$ ,  $\text{O}_2$ ,  $\text{H}_2$  / H and  $\text{D}_2$  / D have a direct impact on the NEG coatings in the vicinity of the gas injection point. Loss of pumping capacity and degradation of the NEG-coated surface SEY must be carefully considered. Due to the fact that these gases are pumped by the NEG coating, pollution of the far-away cold surfaces is less likely to be a limiting factor, although this should be checked by detailed simulations on a case-by-case basis. Nitrogen and oxygen are chemisorbed at the surface of the NEG coating. The pumping sites are gradually occupied by chemisorbed molecules, which results, after some exposure to a saturation of the surface and, as a first consequence, a direct reduction of the pumping capacity. The surface capacity of a rough NEG surface for nitrogen is about  $1.5 \times 10^{15}$  molecules/cm<sup>2</sup> [69]. At the considered exposures for fixed-target physics, the SEY properties of the NEG coating is not expected to be substantially affected. A reactivation of the surface properties is possible, though time-consuming, by baking out the beam pipe for a long enough time at the chosen and high enough temperature [69]. By this process the sticking atoms are diffused into the bulk of the NEG coating. A degradation of the pumping speed is observed after a certain number of cycles. The maximum possible number of cycles is reached when the solubility limit is attained (which depends on the type of gas) [69].

The injection of hydrogen (or deuterium) gas requires special attention due to the fact that, even at room temperature, this gas diffuses into the NEG bulk. This results in a large pumping capacity, but also in a possible embrittlement of the thin coating. The embrittlement limit for hydrogen in commercial NEG is about 25 mbar  $\ell/\text{g}$  [70]. A safe margin for TiZrV films is approximately 4 mbar  $\ell/\text{g}$  [71]. The nominal thickness of LHC beam pipe NEG coatings being  $2\ \mu\text{m}$  and considering the mass density around  $5.5\ \text{g}/\text{cm}^3$ , an estimate of the limit imposed by embrittlement can be obtained for the specific case of a hydrogen gas injection. A molecular flow simulation should be performed to quantify the amount of hydrogen absorbed by the NEG coatings in the vicinity of the target.

When using a storage cell in the LHC, the surface exposed to the beams must be coated with

<sup>5</sup>A “getterable” gas is a gas that is efficiently pumped by NEG.

suitable materials in order to mitigate possible beam-induced desorption or electron cloud effects. In the case of unpolarised noble gases, a NEG coating could be considered. If getterable gases are also considered as target, an implementation with carbon coating should be investigated. For polarised targets, the additional requirement to preserve nuclear polarisation imposes further constraints. At HERMES [14], the storage cell was cooled to approximately 100 K and a light water vapour admixture added to the atomic beam, which formed a thin ice coating on the storage cell. This coating was used to strongly inhibit hydrogen recombination, thereby preserving also a high target nuclear polarisation. Water exhibits a rather high SEY value [72]. Implementation of a polarised hydrogen/deuterium gas target in the LHC using the storage cell technique will therefore require an R&D program to demonstrate that a suitable coating, compatible with both LHC and target requirements, can be found.

Gas ionization by the beam and wall surface bombardment may produce both electrons and ions. Photo-induced emission at the LHC (in particular from synchrotron radiation) may also produce electrons. These mechanisms depend on the beam type, beam parameters, the vacuum pressure, the properties of the exposed wall surfaces (roughness, material type, coverage, etc.). Simulation codes have been developed (e.g. VASCO [73], PyELOUD [74]) that may help to predict the ion or electron build-up effects of a given gaseous fixed-target design. Simulation studies have been made for the SMOG upgrade and are briefly discussed in Section 4.6 below.

## 4.2 Beam life time and local beam losses

The beam losses at the gas target could have an impact on the beam life time and on integrated luminosity of other experiments. The life time reduction can be estimated by calculating the beam-gas interaction loss rate of a bunch population  $N$  due to the gaseous target

$$\frac{dN}{dt} = -\Theta f_{\text{rev}} N \sigma_{bg}, \quad (7)$$

where  $\Theta$  is the areal density of the target gas,  $f_{\text{rev}}$  the bunch revolution frequency (approximately 11245 Hz for the LHC) and  $\sigma_{bg}$  is the beam-gas interaction cross section (including all processes that can cause the loss of a beam particle). This rate induces a beam life time  $\tau_{bg}$  by beam-gas losses given by

$$\tau_{bg} = -\frac{N}{dN/dt} = (\Theta f_{\text{rev}} \sigma_{bg})^{-1}. \quad (8)$$

For a 7 TeV proton beam, if one assumes a cross section  $\sigma_{bg} \approx A^{0.7} \sigma_{pp}$  ( $A$  the target atomic mass and  $\sigma_{pp}$  is taken here to be the total proton-proton cross section with a value of approximately 50 mb at the center-of-mass energy  $\sqrt{s} = 115$  GeV), an areal density of  $\Theta = 10^{14}$  nuclei/cm<sup>2</sup> causes a  $\tau_{bg}$  in the range from 8.5 days for xenon to 250 days in case of hydrogen. As a consequence, the impact of gas targets on the beam life time, in the range of considered target types and areal densities, is negligible. However, other limitations may come from the impact on the machine caused by the local beam-gas losses. In some cases, these loss products can propagate to cold machine elements and induce a quench or cause radiation damage to equipment. These effects must be carefully taken into account.

A first study for beam-gas targets at IP8 was performed [76], using HL-LHC parameters (beam intensity of  $6.07 \times 10^{14}$  protons) which indicates that the local loss rates estimated to quench a magnet at the LHC design stage are reached at  $\Theta \approx 2 \times 10^{14}$  nuclei/cm<sup>2</sup> for hydrogen. The corresponding luminosity is  $1.36 \times 10^{33}$  cm<sup>-2</sup>s<sup>-1</sup>. For xenon (should such a gas be usable in the LHC) the limit is at  $\Theta \approx 1.2 \times 10^{13}$  nuclei/cm<sup>2</sup>. The study also showed that the limits are rather insensitive to the position of the storage cell which was placed at  $z = -1.5$  m and  $z = -3$  m. Figure 22 shows, as an example result of these simulation studies, the loss spectrum for LHC beam 1 (at 7 TeV energy) passing through a  $10^{14}$  nuclei/cm<sup>2</sup> thick hydrogen target at  $z = -1.5$  m from IP8 (located near  $s = 23315$  m). A pessimistic estimate of the quench limit on the induced heat dissipation, used during the LHC design, is 8.7 W/m. It is known today that the real quench limit is likely higher and also that it depends on the



distribution of the power in the coils. The quoted limitations on the gas densities should therefore be considered as conservative and could be refined in the future through further energy deposition studies of the most exposed magnets.

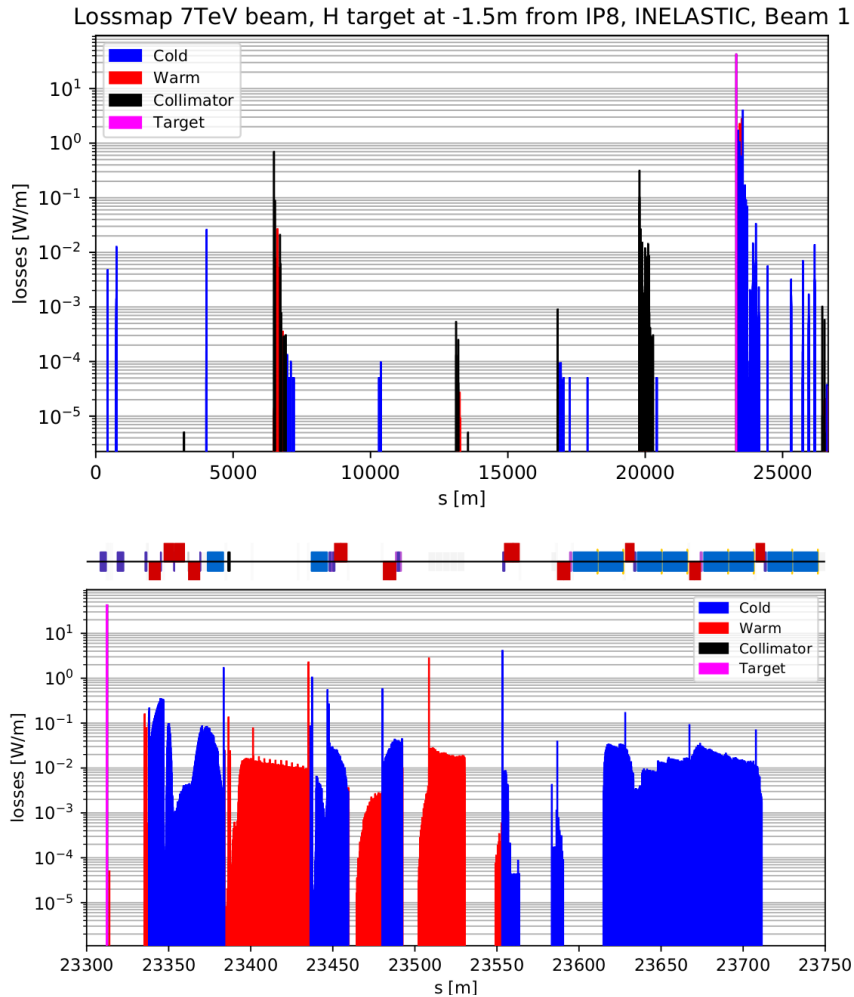


Fig. 22: Loss distribution around the LHC, as simulated with the SixTrack-FLUKA couplings [75] due to inelastic interactions with a  $10^{14}$  nuclei/cm<sup>2</sup> thick hydrogen target at -1.5 m from IP8 (for beam 1 at 7 TeV energy, with nominal HL-LHC intensity). Maximum cold losses: 4.105 W/m at  $s = 23553.4$  m. The bottom graph shows a zoomed region on the right of IP8. Bin width set to 10 cm. Figure taken from [76].

In the case of Pb beams, the beam-gas interaction cross section is considerably larger, but the induced life time reduction may still be kept at an acceptable level by reducing the gas density. In this case, some processes specific to ion collisions (such as bound-free pair production) may cause intense local losses in areas of the insertion region. Dedicated simulation studies of beam-gas losses are required to define limits on the areal density of gas targets with ion beams.

### 4.3 Storage cell principle

The use of a tubular storage cell coaxial with the beam allows to maximize the areal density seen by the beam given a certain gas input flow. The storage cell principle, and its genesis, has been described extensively in Ref. [77] and has been used in several storage rings since the 1980's. Gas is injected in the middle of an open-ended tube, see the sketch in Fig. 23, and a particle beam traverses the tube. If the source of gas is in the form of an atomic beam (like in the case of polarised hydrogen or deuterium),

the atoms reach the center of the storage cell ballistically via a feed tube with a diameter of dimension comparable to that of the storage cell diameter (middle sketch of Fig. 23). In all other cases, the feed tube is a capillary of negligible vacuum conductance when compared to the storage cell. Before escaping the cell, the atoms or molecules undergo a large number of wall encounters, which enhances the density on the beam path. The resulting density profile  $\rho(z)$ , with  $z$  along the beam axis, is approximately triangular with a maximum  $\rho_{\max}$  in the center (at  $z = 0$ ). Here, one assumes molecular flow. Given an injected gas flux  $\Phi$  and a storage cell geometry as in Fig. 23, then  $\rho_{\max} = \Phi/C$ , where  $C$  is the total gas conductance from the center of the cell. An estimation of  $C$  is obtained (in  $\text{cm}^3/\text{s}$ ) by using the cylindrical tube formula summing over the parallel conductances of the 2 (or 3) tubes of diameter  $d_i$  and length  $L_i$  from the cell center, all measured in cm.

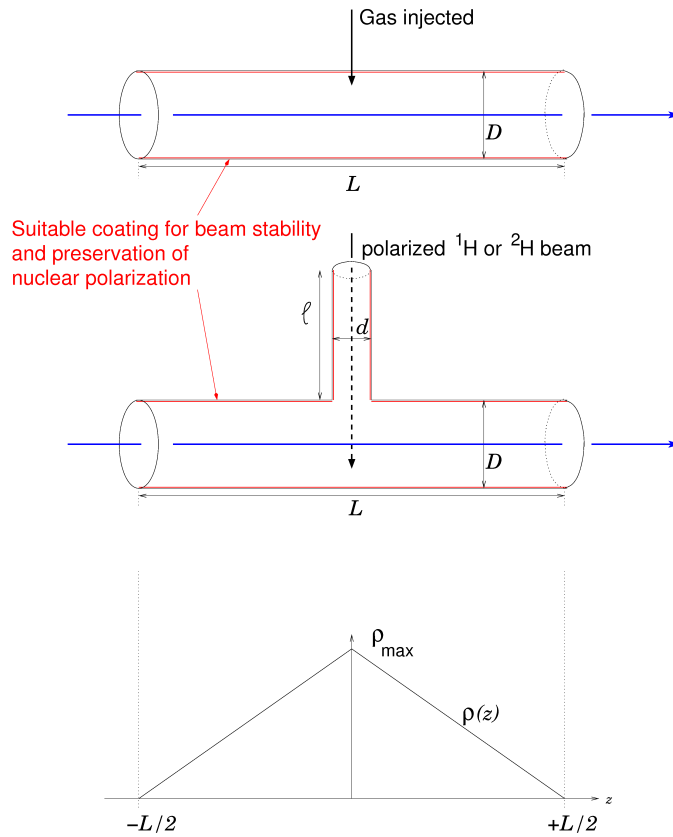


Fig. 23: Principle of storage cell with triangular gas distribution (see e.g. Ref. [77]). Top: typical situation for unpolarised gas (or polarised  $^3\text{He}$ ). Middle: the case with a feed tube for an atomic beam (H, D). Bottom: resulting density profile along the beam axis.

$$C = 3810 \sqrt{\frac{T}{M}} \sum_i \frac{d_i^3}{L_i + 1.33 d_i}, \quad (9)$$

Here,  $T$  is the temperature of the cell (in K) and  $M$  is the gas molecular mass (in unified atomic mass unit). In this simple derivation the areal density is given by  $\Theta = \rho_{\max} L/2$  where  $L$  is the length of the cylindrical tube along the beam path. The resulting beam-gas luminosity  $\mathcal{L}$  per bunch is

$$\mathcal{L} = \Theta f_{\text{rev}} N. \quad (10)$$

Note that the luminosity increases approximately with the inverse third power of the cell diameter. It is therefore crucial to minimize this parameter in order to reach the best figure-of-merit of luminosity

over injected gas flow. For polarised gas targets, due to the limited polarised gas flow intensity, cell temperatures of order of 100 K are often used in order to increase the gas target density by a factor proportional to  $T^{-\frac{1}{2}}$ . The temperature also plays a role in the preservation of the target nuclear polarisation.

#### 4.4 Aperture limitations for storage cells

The insertion of elements such as a storage cell inside the vacuum pipe and close to the beam requires extreme care from many points of view. In particular, the aperture of every element all around the accelerator ring has to be protected by the collimation system in order to guarantee safe operation. As a consequence, a minimum acceptable aperture has to be respected in the design of every element to be installed in the LHC. The minimum safe radius for a storage cell to be inserted inside the vacuum pipe in proximity of IP8 for the HL-LHC machine at 7 TeV has been studied and discussed in detail in Ref. [78]. The main findings are summarized here.

The safe aperture was calculated as a function of the maximum longitudinal distance reached by the cell with respect to IP8, where the optical beta functions and the beam size are minimum. Different experimental configurations and scenarios were taken into account in the calculation of the final minimum radius. The experimental configuration at LHCb was set in order to let the experiment work at a constant luminosity, i.e. leveled throughout every fill. This affects the calculation of the minimum safe storage cell aperture through the separation used for the leveling. The variables to take into account for such a calculation are the optical beta-function at the interaction point,  $\beta^*$ , the parallel beam separation and the presence of both an external crossing angle and the internal spectrometer angle. The cell is supposed to be retractable, in such a way that it would be placed at a transverse position centered around the actual beam position once the beams are colliding and stable beam conditions are achieved. Otherwise, the calculation would be dominated by constraints imposed during particular stages of the fill cycle, such as injection. The calculation thus focused only on the scenario with colliding beams.

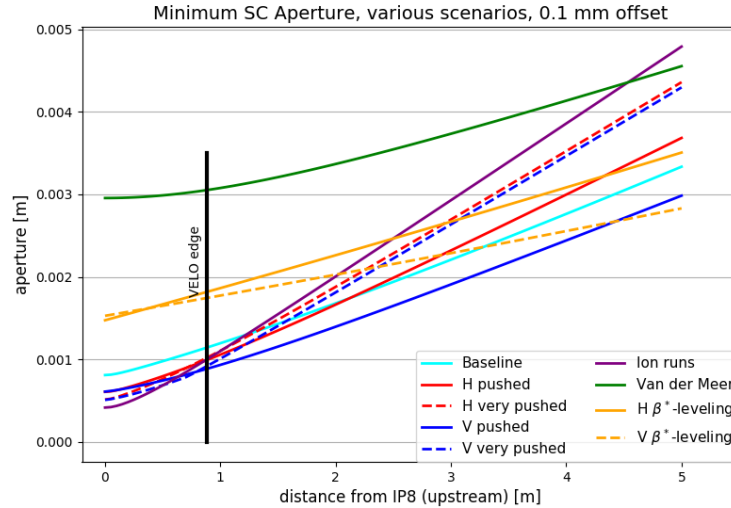


Fig. 24: Minimum storage cell aperture for all considered IP8 scenarios. A 0.1 mm offset due to orbit drifts is assumed (i.e. storage cell re-positioned at every fill). Figure taken from Ref. [78].

As shown in Fig. 24, depending on the distance from IP8, a minimum radius between 3.0 mm and 4.8 mm is found, assuming that the storage cell is realigned in every fill so that it is never misaligned by more than 0.1 mm. The dominating limitation is given by the conditions during the van der Meer scans (luminosity calibration scans) and the vertical crossing configuration with very pushed  $\beta^*$  values. This value gives the minimum aperture, after all tolerances on the storage cell itself have been subtracted,

such as manufacturing and alignment tolerances. The design aperture of a storage cell should thus be correspondingly larger than this minimum acceptable radius.

### 4.5 Impedance and wake fields

Bunched beams with 40 MHz bunch frequency and high bunch charge represent strong sources of electromagnetic radiation. The general rules for guiding these beams safely from the impedance point of view are to (i) increase the distance to the beam, provide maximum possible conductivity of the surrounding surfaces and reduce the dielectric and magnetic losses of the surrounding materials in order to minimize the resistive-wall contribution; (ii) avoid the introduction of cross-sectional changes and if cross-sectional changes are introduced, make their surrounding surfaces well conducting and vary their shape as smoothly as possible; finally, (iii) avoid excitation of cavity-like structures, antenna-like protrusions or other resonating geometries, which is usually achieved by minimizing unnecessary empty volumes and shielding those volumes, which cannot be avoided. The ideal accelerator device from impedance point of view is therefore a smooth, perfectly conducting, vacuum pipe with a large enough radius, and which is actively cooled. Depending on the functional specifications of the device, a specific suitable trade-off between the various impedance contributions (real/imaginary parts, low frequency/high frequency contributions, longitudinal/transverse beam impedances, as well as broadband/narrow band resonator contributions). Said specifications are to be found explicitly for each device.

Nevertheless one can draw the following general guidelines:

- Moveable devices in LHC usually need to approach the beam closer than standard devices, and special care needs to be taken to increase the conductivity of the surfaces, check that potential anti-electron cloud coatings do not degrade beam stability, and check that there is sufficient cooling. As a general rule, all near-beam equipment should be actively cooled.
- In most cases, resonances at lower frequencies (i.e. below 1 GHz) have a much larger impact on stability and heating than resonances at higher frequencies. Such resonances can be created for instance by an antenna larger than 7.5 cm or a cavity of radius larger than 10 cm. More complex geometries such as Roman pots also present low resonant frequencies due to resonances along characteristic lengths of the geometry (here along the perimeter of the Roman pot). Materials with large dielectric and permeability constants also decrease resonant frequencies and should be avoided for near beam applications in general, unless their magnetic losses are intentionally used to reduce the quality factors of some resonances. It is therefore crucial to provide very compact designs, removing all unnecessary vacuum volumes, and shielding moving mechanisms as well as volumes that cannot be made transparent for beam impedance with the use of RF fingers or other mitigation. Finally, any abrupt steps should be tapered.
- Optimizing the impedance of the moveable device in parking position is a priority since the detrimental impact of impedance on beam stability is maximum (i) at low energy – due to the lower beam rigidity –, (ii) high intensity, and (iii) before head-on collisions that provide additional Landau damping.

Validation of the design with simulations, bench measurements – to identify non-conformities and shielding issues –, and machine protection intensity ramp-up steps in the LHC allow for the use of moveable devices in LHC.

The case of an openable storage cell in the LHC, was studied in detail in the context of the SMOG upgrade (SMOG2 project) see Section 4.6.

### 4.6 SMOG upgrade (SMOG2)

A proposal has been made to upgrade the fixed-target luminosity obtained with SMOG at LHCb (IP8) by injecting the gas in a storage cell attached to the upstream end of the VELO RF shields, as depicted

in Fig. 25, taken from Refs. [79, 80]. The cell must be split in two halves in order to respect the LHC injection aperture requirement of about 50 mm minimum diameter. When closed the cell radius is limited by LHC aperture requirements and possible background rates to the LHCb detector originating from beam-halo interactions.

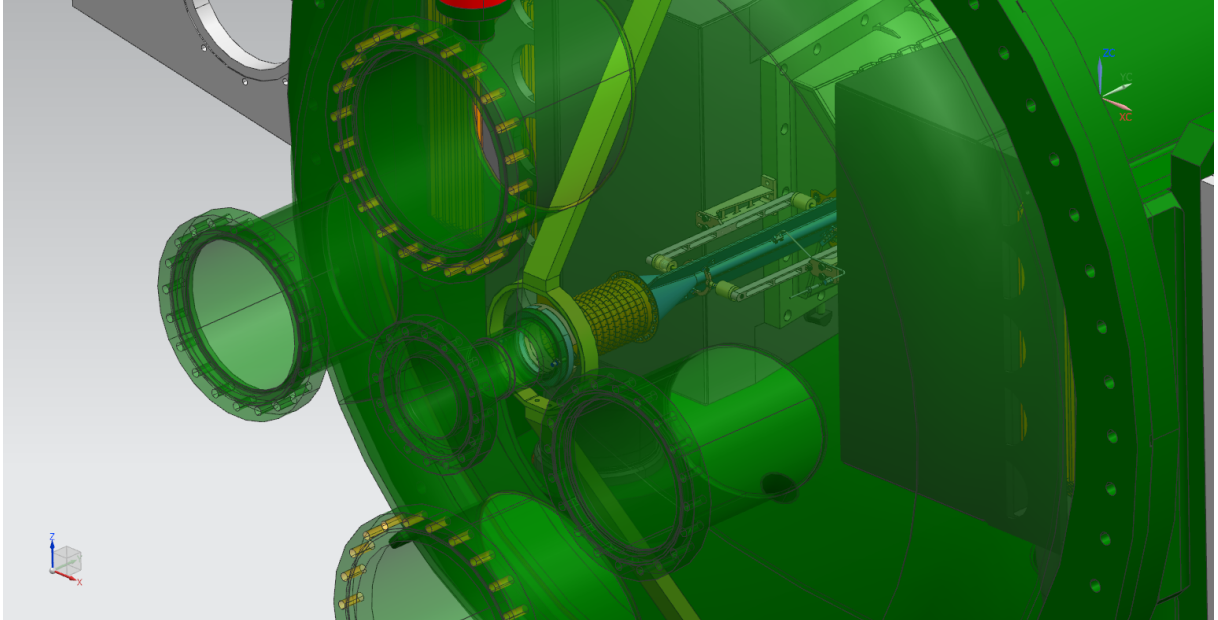


Fig. 25: A proposed implementation of an openable storage cell in LHCb to increase the unpolarised gas target thickness. Only one half is shown, for clarity. Global view with VELO detector boxes. *Courtesy of V. Carassiti (INFN Ferrara).*

The SMOG2 cell will increase the capability of LHCb to perform fixed-target experiments. As an example, the He density during the 2016 SMOG run [57] was approximately  $6.5 \times 10^9$  He/cm<sup>3</sup> with an injected flux of  $3.6 \times 10^{15}$  He/s. Using a storage cell with a diameter of 1 cm and a full length of 20 cm, with the same He flux, one would obtain a central density of  $\rho_{\max} \approx 6.2 \times 10^{11}$  He/cm<sup>3</sup>. Considering the longitudinal vertex position integration, an enhancement of the target thickness by about a factor of 12 can be obtained with the storage cell when compared with the current SMOG setup. Larger enhancement factors are obtained for heavier gases.

A detailed study of the SMOG2 implementation was carried out and documented in Refs. [79, 80]. Here, the main features are briefly summarized.

#### 4.6.1 SMOG2 design

The storage cell assembly inside the VELO vessel is shown in Fig. 25. It consists of two halves that are moved together with the VELO halves. Further details are shown in Fig. 26: coming from upstream (left of IP8) the system is composed of a wake field suppressor, a conical shape, the storage cell proper (an open-ended tube with wings) and a contact piece between the cell and the VELO RF boxes. The wake field suppressor and contact piece are made of 75  $\mu\text{m}$  thick CuBe to guarantee flexibility and low mass while providing good electrical contact. They are provided with gaps for pumping the injected gas away from the beam path. The conical shape allows for a smooth transition from the upstream beam pipe diameter (56 mm) to the cell tube diameter (10 mm). The storage cell proper has length of 20 cm, a diameter of 1 cm (in closed position) and consists of 0.2 mm thick 99.5% pure aluminium machined out of a block with 20  $\mu\text{m}$  accuracy. The side wings are required to guarantee good flow resistance when in closed position. A spring mechanism in the supporting hinges of one half allows for an optimal closure between the opposing faces of the two halves. More details can be found in Refs. [79, 80]. Extensive

robustness tests have been performed on a prototype system and will be repeated with the final assembly before installation in the LHC.

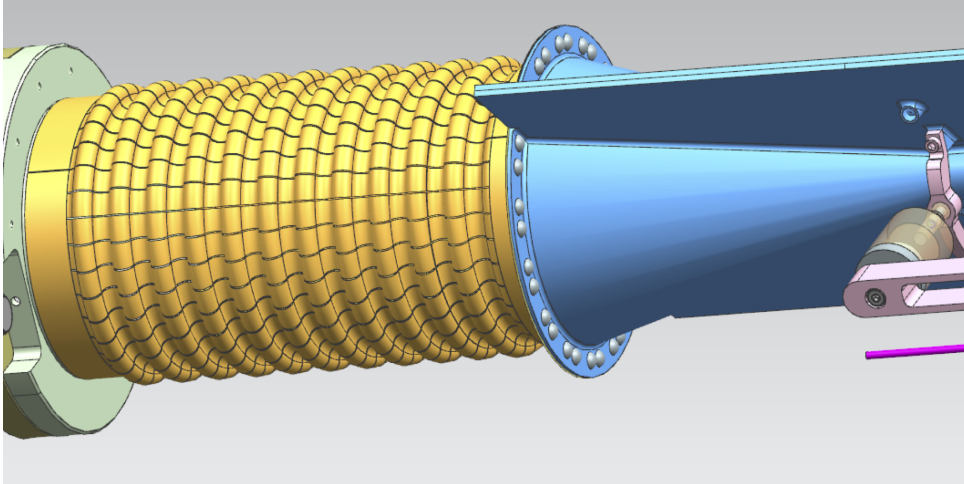


Fig. 26: Detail of the proposed implementation of an openable storage cell system in LHCb. Left: in yellow, upstream wake field suppressor in closed position. Right: in blue, tapered part of the storage cell. *Courtesy of V. Carassiti (INFN Ferrara).*

The cell temperature will be monitored in real time by a set of thermometers. This is required both to calculate the gas density seen by the beams and to monitor heat dissipation from beam-induced ohmic losses and bombardment losses. The gas is injected in the cell center by means of a solid Al capillary, itself connected to a long stainless steel tube that interfaces to the external gas feed connection. A gas-feed system has been designed that will allow to switch in real time between different gas types and which will provide a calibrated measurement of the injected gas flow. It will be combined with the cell temperature measurement and gas molecular flow simulation results to obtain a gas density profile, itself used for luminosity determination.

#### 4.6.2 Machine interface issues

The implementation of a movable device in the LHC for use at nominal beam intensity always requires a careful design that respects the LHC collimation hierarchy, aperture constraints and machine protection guidelines. In the case of SMOG2, a detailed investigation of the aperture constraints for the different beam configurations at IP8 of future LHC runs was carried out [78]. The SMOG2 storage cell assembly is designed such as to be always in a more retracted position as compared to the VELO RF boxes. For this reason, and because the storage cell halves moves with the VELO, protection against failure scenarios relies on the same mechanism as the VELO protection, i.e. a sufficient aperture margin during standard operation and a fast detection of failures by the Beam Conditions Monitor (BCM) followed by a triggered beam dump request.

Wake field and resonant mode simulations, as well as validation measurements on a mock-up setup, were performed with the modified VELO design, taking into account the SMOG2 [81]. The main conclusions are as follows:

- The additional contribution to the low frequency broadband impedance due to the SMOG2 remains small compared to the baseline VELO wake field suppressor scheme; as a consequence, with this information, LHC longitudinal and transverse beam stability is not expected to be altered significantly.
- There is no indication that the addition of the SMOG2 alters longitudinal and transverse resonant modes significantly in both open and closed positions.



- In the open position, some resonant modes have been identified which could result in a non-negligible heat dissipation if the beam spectrum couples to the mode. The analysis of the heating revealed that the overall heating, due to the complete beam spectrum, would be driven by individual modes striking the beam spectrum lines, whereas the total heating due to the remainder of the modes was not as significant. In this worst case scenario, in which the individual resonant mode are shifted manually to strike a beam spectral frequency line, two modes in particular could potentially deposit non-negligible amounts of power on the SMOG2 cell. The first mode at 326 MHz, if it were to shift by 6.12 MHz, would produce nearly 14 W (out of a total of about 820 W in the entire structure) of heating on the SMOG2 Cell. A second mode at 365 MHz, shifted by 4.44 MHz would produce nearly 10 W (out of a total of about 450 W) on the SMOG2 cell. Note that these values could increase by up to a factor 4 in case the electromagnetic fields generated by the interaction of the two counter-rotating beams with the cavity add up in phase.
- In the closed position, given the smooth transitions of the geometry, the main effect will be the mirror current resistive losses, which is calculated to be 4 W [79], and considered an acceptable power deposition. Resonant heating into the closed cell is not to be expected if the geometry remains conform to the design.
- The RF measurements performed with a VELO mockup [81] highlighted the importance that the structure is mechanically robust and keeps its design shape throughout LHC operation.

It has been estimated that, in the conservative case that no heat is extracted by bulk conductivity from the storage cell, a power of 30 W dissipated equally in the two storage cell halves would result in a temperature increase of 61 K, limited by radiative cooling [79].

The interaction of the beam with large gas densities can lead to beam instabilities due to the ionization of the gas molecules. This effect was observed in the LHC and in particular in the 16L2 half-cell, where an accidental gas inlet took place in 2017 [68, 82]. Considering that the integrated gas densities foreseen with SMOG2 are at least two orders of magnitude lower than estimated in 16L2 [83] and that the beta-function at the location of the cell is at least an order of magnitude smaller, similar fast instabilities are not expected to occur. Preliminary simulation studies of the beam-induced ionization and the resulting electron and ion distribution in a storage cell have been performed [84] considering a single circulating beam. Based on the performed studies, instabilities are not expected with the foreseen gas densities for light gases, such as H and H<sub>2</sub>. For heavy gases, such as Xe, higher electron and ion densities build up for a given gas density. To confirm that the injection of such gases is viable from the point of view of beam stability, further studies should be performed. The impact of the secondary electron yield (SEY) of the cell surface on the electron and ion distributions has also been considered. A lower SEY leads to lower densities of electrons for a given gas density and thus provides more margin for beam stability. In the case of heavy gases, also the heat load deposited on the cell walls can be high with the foreseen gas density, if the SEY is high. It should be noted that, in the absence of a low-SEY surface, detrimental build-up of electron clouds through multipacting could occur when the cell is in the open position and no gas is injected. For this reason the SMOG2 storage cell will be coated with a low-SEY amorphous carbon coating.

#### 4.7 A polarised H/D target at the LHC

A polarised gas target (PGT) implementation at the LHC, using the well established Atomic Beam Source (ABS) technique combined with a storage cell and associated polarimetry, is being studied by a group of people [85–87]. The conceptual sketch of a proposed PGT arrangement upstream of the LHCb VELO is shown in Fig. 27. The positions of each element are indicated in mm from the colliding-beams interaction point (IP8) which itself is within the VELO detector at  $z = 0$ . In the figure one sees from right to left: a new sector valve, a target chamber with two conical wake field suppressors, WFS1 and WFS3 (both about 20 cm long), a cold storage cell (30 cm, in blue) with its perpendicular feed tube for injection of an atomic beam, surrounded by a magnet (in green) providing a transverse guide field  $B_0$  of about 0.3 T,

#### 4. Gaseous targets

a tracker (in red) around a 1 cm aperture perforated tube (WFS2, 15 cm long). The different pumping stages are indicated. The retractability of the (split) components is denoted with black arrows.

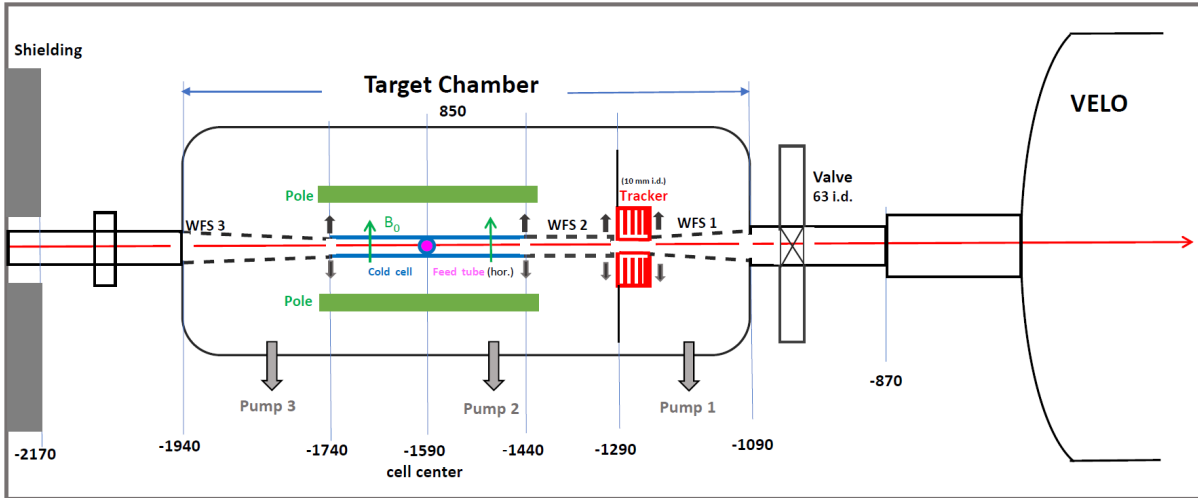


Fig. 27: A conceptual sketch of a proposed polarised hydrogen/deuterium gas target at LHC IP8 (LHCb). Description in the text. Figure taken from Ref. [85].

The main challenge for this implementation will be to identify and validate a suitable storage cell wall coating that preserves both a high target nuclear polarisation and smooth LHC operation. An ultrathin ice coating (as the one used in the HERMES experiment [14]) is currently under investigation in a dedicated R&D project. An alternative design without storage cell, using only a (possibly inclined) polarised atomic beam, could also be considered, but would result in a lower areal density and luminosity.

A few other interesting challenges have already been addressed in the WG discussions.

The effect of peaked flow (unrestricted by the storage cell walls), and its impact on the vacuum system, has been estimated. It can be kept under control by use of adequate conductance limiters [88]. For a windowless gas target based on a storage cell like this PGT, about 42% of the flow is emitted back towards the ABS, and about 29% each is emitted as a peaked flow from the upstream and the downstream end of the beam tube. The upstream flow has to be pumped such as to minimize the flow to LHC beam tube and eventually to the cold elements located at  $\sim 20$  m upstream. The downstream flow might partially enter the VELO detector vessel and put a significant load on the VELO vacuum system. By analytical calculation, it is possible to calculate that only about 0.34% of the flow emitted downstream towards the VELO vessel passes a 10 mm diameter orifice, which indicates that efficient differential pumping could be implemented in such a PGT. Moreover, during a run of  $\sim 10^6$  s and if no other gas components would enter the VELO vessel, its vacuum system would be loaded by a quantity as low as 1 mbar  $\ell$  of hydrogen ( $H_2$ ).

The effect of beam-induced depolarisation by RF fields has also been considered [89]. Depolarisation by the bunch fields of the stored beam has been observed and studied at the HERA Electron Ring by the HERMES experiment. Based on these results, a preliminary estimate has been performed of the effects of the LHC beam on a polarized hydrogen gas target. The main differences come from the bunch frequency and the longitudinal bunch profile. It is possible to conclude that resonant depolarisation at the LHC via the  $\sigma_{2-4}$  transition seems to be negligible, compared with HERA, despite the 25 times higher beam current. The other transitions affecting the target polarisation ( $\pi_{1-2}$  and  $\pi_{3-4}$ ) have a much wider spacing and can be avoided by proper choice of the guide field.

In case of an implementation at IP8, the space availability in the VELO alcove needs to be studied. If required, some space could be gained by moving along the beam axis the upstream corrector magnet (MBXW), or by replacing it with a more compact one, and displacing as well the removable shielding.



Given the challenges and amount of studies to be performed, an installation of a PGT could be envisaged in LS3 at the earliest.

## 5 Summary and conclusions

The Physics Beyond Colliders Fixed-Target working group has investigated the feasibility and impact on the LHC machine of several fixed-target physics proposals. The effort focused on the projects that, given the context of the LHC programme, were the most advanced and/or the most supported by the physics community.

The use of bent crystals for deflecting a fraction of the beam halo and transporting it to an off-axis solid target was considered and a few specific implementations were studied. The most mature of these studies includes a first crystal  $\sim 100$  m left of IP8 and a tungsten target followed by a second bent crystal at  $\sim 1$  m left of IP8. The second crystal is used to channel baryons produced in the target in order to measure their dipole moment (magnetic or electric). In order to match the LHCb angular acceptance, this second crystal must have a bending angle of at least  $\sim 14$  mrad, which imposes also a length of  $\sim 5$ – $10$  cm. This was identified as an important and non-trivial feature to be verified on a prototype with a high-energy particle beam. Testbeam experiments at the SPS North Area were carried out by the proponents and demonstrated that, indeed, acceptable channeling efficiencies (more than  $\sim 12\%$  at 180 GeV) are achievable even with such crystal parameters. Although the extrapolation of the performance to LHC energies leaves room for some uncertainty, the results are very promising. The IP8 layout was optimized and it was shown that it could deliver at least  $\sim 10^6$  *PoT/s* while being compatible with high intensity LHC physics operation, provided the host experiment (LHCb) can tolerate the additional interactions from the target system. A number of promising handles to increase the signal yield have been identified (Ge versus Si crystal type, target length, controlled excitation of beam losses for selected bunches) and some would require further studies to be confirmed and/or optimized. An absorber layout right of IP8 and LHCb has been sketched, but more in-depth studies are required to complete the design and assess other potential impacts on the machine due to the disposal of the surviving protons.

A similar implementation without the second crystal could be used for fixed-target operation with a variety of solid targets and with the proton and lead beams. This would allow one to probe the quark-gluon plasma and hadronic matter in uncharted kinematic domains and would provide important inputs to cosmic ray physics. An initial study for such a scheme at IP2 was carried out with an internal retractable solid target. A complete study of the proposed layout as done for the IP8 scheme is now required in order to assess the feasibility and the achievable flux in IP2 with the proton beam and the feasibility with the lead beam. In parallel, studies in ALICE are needed to establish the physics performance. This setup is under investigation in ALICE.

An installation at Point 8 of a bent crystal setup for physics could, if well prepared, take place in a year-end technical stop of the LHC machine (during Run 3). In Point 8 a new vacuum sectorization is being installed in LS2 in order to enable an installation of equipment in the section just upstream of the VELO vacuum vessel without requiring an LHCb VELO and beam pipe bake-out. For Point 2, an installation in LS3 could be considered.

The effective use of a gaseous target in the LHC was already demonstrated at LHCb using the SMOG system (with He, Ne and Ar gas targets). The PBC fixed-target working group considered a proposal to boost the usage of the injected gas by implementing a cylindrical storage cell in front of the LHCb VELO (SMOG2 proposal). Compared to SMOG, one or two orders of magnitude in areal density can be gained for the same gas flow. A detailed design study was presented and critical machine and detector interface aspects—impedance, dynamic vacuum, beam aperture, beam losses, machine and experiment protection—were reviewed. (impedance, dynamic vacuum, beam aperture, beam losses, machine and experiment protection). The resulting design reached sufficient maturity to be considered for installation in LS2. The setup is currently being prepared for installation, aiming at first usage of SMOG2 in the early phase of Run 3. The types and quantities of gases that will be used (beyond the

already tried He, Ne and Ar gas flows) are yet to be reviewed. The getterable gases H<sub>2</sub>, D<sub>2</sub>, N<sub>2</sub> and O<sub>2</sub> have been mentioned, as well as the heavier noble gases Kr and Xe. The potential impact on the machine of these gases (NEG coating degradation, condensation on cold surfaces) is yet to be studied and quantified.

The storage cell technique implemented for SMOG2 appears also in the polarised target proposal presented to the working group. Here, an atomic beam source would be used to inject polarised hydrogen or deuterium into the feed tube of the storage cell, allowing one to study the nucleon spin structure. The question of nuclear polarisation preservation, by a suitable surface coating, has been identified as the most important challenge, requiring R&D. This challenge is being addressed by the proponents as a first step toward future more detailed implementation studies. Installation of a polarised gas target is not foreseen before LS3.

### Acknowledgements

We wish to thank Giacomo Graziani (from the QCD PBC working group) for providing a list of likely candidate gas types for the gaseous fixed-target physics program. Individual authors of this report have received financial support from ERC Ideas Consolidator Grant No. 771642 SELDOM (European Union). The studies for the ALICE fixed target proposal were supported in part by the RFBR/CNRS joint grant 18-52-15007/PRC-1980 and have received funding from the European Union's Horizon 2020 research and innovation programme under grant agreement No 824093.

### References

- [1] O. Brüning *et al.* (eds), “LHC design report,” Vol. I, CERN, Geneva, Switzerland, CERN Yellow Reports: Monographs. CERN-2004-003-V-1, 2004 [doi:10.5170/CERN-2004-003-V-1](https://doi.org/10.5170/CERN-2004-003-V-1).
- [2] “Kickoff meeting for the Physics Beyond Collider study, 6–7 Sept. 2016,” <https://indico.cern.ch/event/523655>. See also <https://cern.ch/pbc>.
- [3] D. Mirarchi, A.S. Fomin, S. Redaelli and W. Scandale, “Layouts for fixed-target experiments and dipole moment measurements of short-living baryons using bent crystals at the LHC,” [arXiv:1906.08551](https://arxiv.org/abs/1906.08551) [physics.acc-ph], submitted to *Eur. Phys. J. C*.
- [4] D. Mirarchi, S. Redaelli, R. Rossi, W. Scandale, “Experience with multi-TeV beam channeling and crystal extraction at the LHC,” pres. at the Kickoff meeting for the Physics Beyond Collider study, 6–7 Sept. 2016, <https://indico.cern.ch/event/523655>.
- [5] L. Burmistrov *et al.*, “Measurement of short living baryon magnetic moment using bent crystals at SPS and LHC,” expression of interest, CERN-SPSC-2016-030 ; SPSC-EOI-012, <https://cds.cern.ch/record/2194564>.
- [6] A.S. Fomin *et al.*, “Feasibility of measuring the magnetic dipole moments of the charm baryons at the LHC using bent crystals,” *JHEP* **2017** (2017) 120, [doi:10.1007/JHEP08\(2017\)120](https://doi.org/10.1007/JHEP08(2017)120), [arXiv:1705.03382](https://arxiv.org/abs/1705.03382) [hep-ph].
- [7] F.J. Botella *et al.* “On the search for the electric dipole moment of strange and charm baryons at LHC,” *Eur. Phys. J. C* **77** (2017) 181, [doi:10.1140/epjc/s10052-017-4679-y](https://doi.org/10.1140/epjc/s10052-017-4679-y), [arXiv:1612.06769](https://arxiv.org/abs/1612.06769) [hep-ex].
- [8] E. Bagli *et al.*, “Electromagnetic dipole moments of charged baryons with bent crystals at the LHC,” *Eur. Phys. J. C* **77** (2017) 828, [doi:10.1140/epjc/s10052-017-5400-x](https://doi.org/10.1140/epjc/s10052-017-5400-x), [arXiv:1708.08483](https://arxiv.org/abs/1708.08483) [hep-ex].
- [9] Y. Genolini, D. Maurin, I.V. Moskalenko, M. Unger, “Current status and desired accuracy of the isotopic production cross sections relevant to astrophysics of cosmic rays I. Li, Be, B, C, N,” *Phys. Rev. C* **98** (2018) 034611, [doi:10.1103/PhysRevC.98.034611](https://doi.org/10.1103/PhysRevC.98.034611), [arXiv:1803.04686](https://arxiv.org/abs/1803.04686) [astro-ph.HE];

- M. Korsmeier, F. Donato, M. Di Mauro, “Production cross sections of cosmic antiprotons in the light of new data from NA61 and LHCb experiments,” *Phys. Rev. D* **97** (2018) 103019, [doi:10.1103/PhysRevD.97.103019](https://doi.org/10.1103/PhysRevD.97.103019), [arXiv:1802.03030](https://arxiv.org/abs/1802.03030).
- [10] L. Massacrier *et al.*, “Physics perspectives with AFTER@LHC (A Fixed Target Experiment at LHC),” *EPJ Web Conf.* **171** (2018) 10001, [doi:10.1051/epjconf/201817110001](https://doi.org/10.1051/epjconf/201817110001);  
C. Haddjidakis *et al.*, “A fixed-target programme at the LHC: physics case and projected performances for heavy-Ion, hadron, spin and astroparticle studies,” [arXiv:1807.00603 \[hep-ex\]](https://arxiv.org/abs/1807.00603).
- [11] J.D. Bjorken *et al.*, “Community support for a fixed-target programme for the LHC,” input to the European Particle Physics Strategy Update 2018-2020, [CERN-ESPP-Note-2018 \(contribution 67\)](https://arxiv.org/abs/1807.00603).
- [12] F. Galluccio *et al.*, “Physics opportunities for a fixed-target programme in the ALICE experiment,” input to the European Particle Physics Strategy Update 2018-2020, [CERN-ESPP-Note-2018 \(contribution 47\)](https://arxiv.org/abs/1807.00603), [CERN-PBC-Notes-2019-004](https://arxiv.org/abs/1807.00603).
- [13] A. Bursche *et al.*, “Physics opportunities with the fixed-target program of the LHCb experiment using an unpolarized gas target”, [CERN-LHCb-PUB-2018-015](https://arxiv.org/abs/1807.00603).
- [14] A. Airapetian *et al.* [HERMES Collaboration], “The HERMES polarized hydrogen and deuterium gas target in the HERA electron storage ring”, *Nucl. Instrum. Meth. A* **540** (2005) 68, [doi:10.1016/j.nima.2004.11.020](https://doi.org/10.1016/j.nima.2004.11.020), [arXiv:physics/0408137 \[physics\]](https://arxiv.org/abs/physics/0408137).
- [15] C. Hast *et al.*, “Test of internal Halo targets in the HERA proton ring”, *Nucl. Instrum. Meth. A* **354** (1995) 224, [doi:10.1016/0168-9002\(94\)01015-3](https://doi.org/10.1016/0168-9002(94)01015-3).
- [16] D. Chen, I.F. Albuquerque, V.V. Baublis *et al.*, “First observation of magnetic moment precession of channeled particles in bent crystals”, *Phys. Rev. Lett.* **69** (1992) 3286, [doi:10.1103/PhysRevLett.69.3286](https://doi.org/10.1103/PhysRevLett.69.3286).
- [17] A. Zelenski *et al.*, “Absolute polarized H-jet polarimeter development, for RHIC”, *Nucl. Instrum. Meth. A* **536** (2005) 248, [doi:10.1016/j.nima.2004.08.080](https://doi.org/10.1016/j.nima.2004.08.080).
- [18] K.C. Meehan [STAR Collaboration], “The fixed-target experiment at STAR”, *J. Phys. Conf. Ser.* **742** (2016) 012022, [doi:10.1088/1742-6596/742/1/012022](https://doi.org/10.1088/1742-6596/742/1/012022).
- [19] G. Apollinari, I. Béjar Alonso, O. Brüning, P. Fessia, M. Lamont, L. Rossi and L. Tavian, “High-Luminosity Large Hadron Collider (HL-LHC) : Technical Design Report V. 0.1”, CERN Yellow Report, CERN 2017-007-M, [doi:10.23731/CYRM-2017-004](https://arxiv.org/abs/1706.02266).
- [20] D. Mirarchi *et al.*, “Design and implementation of a crystal collimation test stand at the Large Hadron Collider,” *Eur. Phys. J. C* **77** (2017) 424, [doi:10.1140/epjc/s10052-017-4985-4](https://doi.org/10.1140/epjc/s10052-017-4985-4).
- [21] W. Scandale *et al.*, “Observation of Channeling for 6500 GeV/c protons in the crystal assisted collimation setup for LHC”, *Phys. Lett. B* **758** (2016) 129, [doi:10.1016/j.physletb.2016.05.004](https://doi.org/10.1016/j.physletb.2016.05.004).
- [22] V. G. Baryshevsky, “The possibility to measure the magnetic moments of short-lived particles (charm and beauty baryons) at LHC and FCC energies using the phenomenon of spin rotation in crystals”, *Phys. Lett. B* **757** (2016) 426, [doi:10.1016/j.physletb.2016.04.025](https://doi.org/10.1016/j.physletb.2016.04.025).
- [23] A.M. Taratin, “Particle channeling in bent crystal”, *Phys. Part. Nucl.* **29** (1998) 437.
- [24] A.S. Fomin, A.Y. Korchin, A. Stocchi, S. Barsuk and P. Robbe, “Feasibility of  $\tau$ -lepton electromagnetic dipole moments measurement using bent crystal at the LHC”, *JHEP* **03** (2019) 156, [doi:10.1007/JHEP03\(2019\)156](https://doi.org/10.1007/JHEP03(2019)156), [arXiv:1810.06699 \[hep-ph\]](https://arxiv.org/abs/1810.06699).
- [25] J. Fu, M.A. Giorgi, L. Henry, D. Marangotto, F.M. Vidal, A. Merli, N. Neri and J. Ruiz Vidal, “Novel method for the direct measurement of the  $\tau$  lepton dipole moments”, *Phys. Rev. Lett.* **123** (2019) 011801, [doi:10.1103/PhysRevLett.123.011801](https://doi.org/10.1103/PhysRevLett.123.011801), [arXiv:1901.04003 \[hep-ex\]](https://arxiv.org/abs/1901.04003).
- [26] V.G. Baryshevsky, “Spin rotation of ultrarelativistic particles in a crystal,” *Pis'ma Zh. Tekh. Fiz.* **5** (1979) 182, *Sov. Tech. Phys. Lett.* **5** (1979) 73;

- V.L. Lyuboshits, “The spin rotation at deflection of relativistic charged particle in electric field,” *Yad. Fiz.* **31** (1980) 986, *Sov. J. Nucl. Phys.* **31** (1980) 509;
- I.J. Kim, “Magnetic moment measurement of baryons with heavy flavored quarks by planar channeling through bent crystal,” *Nucl. Phys. B* **229** (1983) 251, [doi:10.1016/0550-3213\(83\)90363-2](https://doi.org/10.1016/0550-3213(83)90363-2);
- L. Pondrom, “Report of the Fixed Target Proton Accelerator Group”, in Proc. 1982 Division of Particles and Fields Summer School on Elementary Particle Physics and Future Facilities, Snowmass, Colorado, edited by R. Donaldson, R. Gustafson, and F. Paige (Fermilab, Batavia, 1983), <https://inspirehep.net/literature/185814>.
- [27] H. Louis *et al.*, “DIPOLE-b: direct probe of short-lived particle electromagnetic dipole moments at LHCb,” CERN-LHCb-PUB-2019-011, <https://cds.cern.ch/record/2687346>.
- [28] W. Scandale, “UA9 Status Report for 2018,” CERN-SPSC-2018-031, 2018, <https://cds.cern.ch/record/2643778>.
- [29] S. Montesano on behalf of the UA9 Collaboration, “Testing the double-crystal setup for Physics Beyond Colliders experiments in the UA9-SPS experiment,” in Proc. 9th Int. Particle Accelerator Conf. (IPAC2018), [doi:10.18429/JACoW-IPAC2018-TUPAF043](https://doi.org/10.18429/JACoW-IPAC2018-TUPAF043).
- [30] CERN EDMS document 1839549, “Replacement of one Primary Crystal Collimator (TCPC) in IR7,” LHC-TC-EC-0010 (2018), [doi:10.5281/zenodo.3860048](https://doi.org/10.5281/zenodo.3860048).
- [31] S. Redaelli *et al.*, “LHC collimator controls for a safe LHC operation,” in Proc. 13th International Conference on Accelerator and Large Experimental Physics Control Systems (ICAPELCS2011), pp. 70–73, <http://accelconf.web.cern.ch/AccelConf/icalepcs2011/papers/mommu003.pdf>.
- [32] D. Quartullo *et al.*, “Characterization of the longitudinal impedance of the LHC UA9 goniometer through simulations and RF measurements,” pres. at the 118<sup>th</sup> meeting of the Collimation Upgrade Specification working group (ColUSM, 2019), <https://indico.cern.ch/event/833077>.
- [33] CERN EDMS document 1113402, “Vacuum acceptance tests for LHC collimators,” (2011), <https://edms.cern.ch/document/1113402/2>.
- [34] R. Bruce *et al.*, “Collimation-induced experimental background studies at the CERN Large Hadron Collider,” *Phys. Rev. Accel. Beams* **22** (2019) 021004, [doi:10.1103/PhysRevAccelBeams.22.021004](https://doi.org/10.1103/PhysRevAccelBeams.22.021004).
- [35] R. Aßmann, B. Goddard, E. Vossenber, and E. Weisse, “The consequences of abnormal beam dump actions on the LHC collimation system,” LHC Project Note 293, CERN, <https://cds.cern.ch/record/691845>.
- [36] R. Aaij *et al.*, “Performance of the LHCb Vertex Locator,” *JINST* **9** (2014) P09007, [doi:10.1088/1748-0221/9/09/P09007](https://doi.org/10.1088/1748-0221/9/09/P09007), [arXiv:1405.7808\[physics.ins-det\]](https://arxiv.org/abs/1405.7808).
- [37] V.M. Samsonov, “On the possibility of measuring charm baryon magnetic moments with channeling,” *Nucl. Instrum. Meth. B* **119** (1996) 271, [doi:10.1016/0168-583X\(96\)00348-5](https://doi.org/10.1016/0168-583X(96)00348-5).
- [38] A.S. Fomin *et al.*, “Feasibility of measuring the magnetic dipole moments of the charm baryons at the LHC using bent crystals,” *JHEP* **1708** (2017) 120, [doi:10.1007/JHEP08\(2017\)120](https://doi.org/10.1007/JHEP08(2017)120), [arXiv:1705.03382\[hep-ph\]](https://arxiv.org/abs/1705.03382).
- [39] R. Aßmann *et al.*, “The final collimation system for the LHC,” in: Proc. European Particle Accelerator Conference 2006 (EPAC 2006), pp. 986–988, <https://inspirehep.net/literature/727805>.
- [40] W. Scandale *et al.*, “Optical layout for the measurement of short living baryon magnetic moment using bended crystals at LHC”, pres. at Kickoff meeting for the Physics Beyond Collider study, 6–7 Sept. 2016, [https://indico.cern.ch/event/523655/contributions/2284521/attachments/1332060/2002778/PBC\\_WalterScandale.pdf](https://indico.cern.ch/event/523655/contributions/2284521/attachments/1332060/2002778/PBC_WalterScandale.pdf).

- [41] C. Dong, “The measurement of the magnetic moment of  $\Sigma^+$  using channeling in bent crystals,” FERMILAB-THESIS-1992-40; State University of New York at Albany, 1992, [doi:10.2172/1426684](https://doi.org/10.2172/1426684).
- [42] B. Salvachua *et al.*, “Decomposition of beam losses at LHC,” in Proc. International Particle Accelerator Conference 2017 (IPAC2017), pp. 88–91, [doi:10.18429/JACoW-IPAC2017-MOPAB009](https://doi.org/10.18429/JACoW-IPAC2017-MOPAB009).
- [43] S. Kostoglou *et al.*, “Luminosity, lifetime and modelling,” in 9th LHC Operations Evian Workshop (2019), [https://indico.cern.ch/event/751857/contributions/3259405/attachments/1785393/3237267/paper\\_Luminosity\\_Evian.pdf](https://indico.cern.ch/event/751857/contributions/3259405/attachments/1785393/3237267/paper_Luminosity_Evian.pdf).
- [44] B. Salvachua *et al.*, “Beam losses, lifetime and operational experience at 6.5 TeV”, in International Review of the HL-LHC Collimation System, [pathhttps://indico.cern.ch/event/780182/contributions/3264114/attachments/1793608/2922819/salvachua-2019-02-11.pdf](https://indico.cern.ch/event/780182/contributions/3264114/attachments/1793608/2922819/salvachua-2019-02-11.pdf)
- [45] M. Tanabashi *et al.*, (Particle Data Group), *Phys. Rev. D* **98** (2018) 030001, “The review of particle physics,” [doi:10.1103/PhysRevD.98.030001](https://doi.org/10.1103/PhysRevD.98.030001).
- [46] R. Aßmann, W. Höfle, S. Redaelli, D. Valuch, D. Wollmann, R. Schmidt and M. Zerlauth, “Controlled Transverse Blow-Up of High-energy Proton Beams for Aperture Measurements and Loss Maps,” in Proc. 3rd International Particle Accelerator Conference (IPAC2012), pp. 4059–4061, <https://accelconf.web.cern.ch/IPAC2012/papers/THPPR039.PDF>.
- [47] A.S. Fomin *et al.*, “The prospect of charm quark magnetic moment determination,” *Eur. Phys. J. C* **80** (2020) 358, [doi:10.1140/epjc/s10052-020-7891-0](https://doi.org/10.1140/epjc/s10052-020-7891-0), [arXiv:1909.04654 \[hep-ph\]](https://arxiv.org/abs/1909.04654).
- [48] D. De Salvador *et al.*, “Highly bent (110) Ge crystals for efficient steering of ultrarelativistic beams,” *J. Appl. Phys.* **114** (2013) 154902, [doi:10.1063/1.4824798](https://doi.org/10.1063/1.4824798).
- [49] A. Baurichter *et al.*, “Channeling of high-energy particles in bent crystals - Experiment at the CERN SPS,” *Nucl. Instrum. Meth. B* **164-165** (2000) 27, [doi:10.1016/S0168-583X\(99\)01062-9](https://doi.org/10.1016/S0168-583X(99)01062-9).
- [50] A. Santamaria Garcia *et al.*, “Machine protection from fast crab cavity failures in the High Luminosity LHC,” in Proc. 7th International Particle Accelerator Conference (IPAC2016) pp. 1485–1488, [doi:10.18429/JACoW-IPAC2016-TUPMW025](https://doi.org/10.18429/JACoW-IPAC2016-TUPMW025).
- [51] S. Redaelli *et al.*, “Plans for deployment of hollow electron lenses at the LHC for enhanced beam collimation,” in Proc. 6th International Particle Accelerator Conference (IPAC2015), pp. 2462–2465, [doi:10.18429/JACoW-IPAC2015-WEBB1](https://doi.org/10.18429/JACoW-IPAC2015-WEBB1).
- [52] K. Elsener *et al.*, “Deflection of high-energy beams by channeling in bent silicon crystals,” in Proc. 4th European Particle Accelerator Conference (EPAC ’94), pp. 2385–2387, [https://accelconf.web.cern.ch/e94/PDF/EPAC1994\\_2385.PDF](https://accelconf.web.cern.ch/e94/PDF/EPAC1994_2385.PDF).
- [53] F. Costantini, “LHB: A Fixed target experiment at LHC to measure CP violation in B mesons,” *Nucl. Instrum. Meth. A* **333** (1993) 125, [doi:10.1016/0168-9002\(93\)90193-L](https://doi.org/10.1016/0168-9002(93)90193-L).
- [54] A.B. Kurepin *et al.*, “Charmonium production in fixed-target experiments with SPS and LHC beams at CERN,” *Phys. Atom. Nucl.* **74** (2011) 446, [doi:10.1134/S1063778811030124](https://doi.org/10.1134/S1063778811030124), *Yad. Fiz.* **74** (2011) 467.
- [55] L. Massacrier, “Physics with fixed-target collisions in ALICE,” pres. at the Physics Beyond Colliders Annual Workshop, Nov. 21<sup>st</sup> and 22<sup>nd</sup> 2017, <https://indico.cern.ch/event/644287/contributions/2724478/>.
- [56] M. Butcher *et al.*, “Controller design and verification for a rotational piezo-based actuator for accurate positioning applications in noisy environments,” in Proc. 41st Annual Conference of the IEEE Industrial Electronics Society (IECON 2015), pp. 003887–003892, [doi:10.1109/IECON.2015.7392706](https://doi.org/10.1109/IECON.2015.7392706).



- [57] R. Aaij *et al.* (LHCb Collaboration), “Measurement of antiproton production in p-He collisions at  $\sqrt{s_{NN}} = 110$  GeV,” *Phys. Rev. Lett.* **121** (2018) 222001, [doi:10.1103/PhysRevLett.121.222001](https://doi.org/10.1103/PhysRevLett.121.222001).
- [58] R. Aaij *et al.* (LHCb Collaboration), “First measurement of charm production in fixed-target configuration at the LHC,” *Phys. Rev. Lett.* **122** (2019) 132002, [doi:10.1103/PhysRevLett.122.132002](https://doi.org/10.1103/PhysRevLett.122.132002), [arXiv:1810.07907 \[hep-ex\]](https://arxiv.org/abs/1810.07907).
- [59] SMOG, a System for Measuring the beam Overlap with Gas, described in C. Barschel, “Precision luminosity measurements at LHCb with beam-gas imaging,” CERN-THESIS-2013-301, RWTH Aachen University, 2014, <https://cds.cern.ch/record/1693671>.
- [60] R. Aaij *et al.*, “Precision luminosity measurements at LHCb,” *JINST* **9** (2014) P12005, [10.1088/1748-0221/9/12/P12005](https://doi.org/10.1088/1748-0221/9/12/P12005), [arXiv:1410.0149 \[hep-ex\]](https://arxiv.org/abs/1410.0149).
- [61] C.A. Aidala *et al.*, “The LHCSpin Project,” input to the European Particle Physics Strategy Update 2018-2020, <https://indico.cern.ch/event/765096/contributions/3295757/>, [arXiv:1901.08002 \[hep-ex\]](https://arxiv.org/abs/1901.08002).
- [62] A. Taschner, E. Kohler, H.W. Ortjohann, A.Khoukaz, “High density cluster jet target for storage ring experiments,” *Nucl. Instrum. Meth. A* **660** (2011) 22, [doi:10.1016/j.nima.2011.09.024](https://doi.org/10.1016/j.nima.2011.09.024), [arXiv:1108.2653 \[physics.ins-det\]](https://arxiv.org/abs/1108.2653).
- [63] A. Khoukaz *et al.*, PANDA Collaboration, “Technical design report for the PANDA internal targets,” (2012), RE-TDR-2012-002, GSI Helmholtzzentrum für Schwerionenforschung, <https://panda.gsi.de/publication/re-tdr-2012-002>.
- [64] O. Gröbner, “The LHC vacuum system,” in Proc. 1997 Particle Accelerator Conference (PAC ’97), pp.3542-6, [doi:10.1109/PAC.1997.753269](https://doi.org/10.1109/PAC.1997.753269).
- [65] See for example in P. Costa Pinto *et al.*, “Thin film coatings for suppressing electron multipacting in particle accelerators,” in Proc. 2011 Particle Accelerator Conference (PAC2011), pp. 2096–98, <https://accelconf.web.cern.ch/PAC2011/papers/thobs6.pdf>, and references therein.
- [66] H. Tratnik, N. Hilleret and H. Störi, “The desorption of condensed noble gases and gas mixtures from cryogenic surfaces,” *Vacuum* **81** (2007) 73, [doi:10.1016/j.vacuum.2005.11.064](https://doi.org/10.1016/j.vacuum.2005.11.064).
- [67] J. Barnard, I. Bojko, N. Hilleret, “Measurements of the secondary electron emission from rare gases at 4.2K,” CERN Vacuum Technical Note (1997), [arXiv:1302.2334 \[physics.acc-ph\]](https://arxiv.org/abs/1302.2334).
- [68] J. Jiménez *et al.*, “Observations, analysis and mitigation of recurrent LHC beam dumps caused by fast losses in arc half-cell 16L2,” in Proc. 9th Int. Particle Accelerator Conf. (IPAC2018), pp. 228-231, [doi:10.18429/JACoW-IPAC2018-MOPMF053](https://doi.org/10.18429/JACoW-IPAC2018-MOPMF053).
- [69] P. Chiggiato, P. Costa Pinto, “Ti–Zr–V non-evaporable getter films: From development to large scale production for the Large Hadron Collider,” *Thin Solid Films* **515** (2006) 382, [doi:10.1016/j.tsf.2005.12.218](https://doi.org/10.1016/j.tsf.2005.12.218).
- [70] P. Chiggiato, “Vacuum technology,” pres. at the Joint Universities Accelerator School (JUAS) 2016, <https://indico.cern.ch/event/471931/contributions/1149644/>.
- [71] Private communication, P. Chiggiato.
- [72] V. Baglin *et al.*, “The secondary electron yield of technical materials and its variation with surface treatments,” in Proc. 7th European Particle Accelerator Conference (EPAC 2000), pp. 217–221, <https://accelconf.web.cern.ch/e00/PAPERS/THXF102.pdf>.
- [73] A. Rossi, “VASCO (VAcuum Stability COde): multi-gas code to calculate gas density profile in a UHV system,” (2004) LHC Project Note 341 <https://cds.cern.ch/record/728512>.
- [74] G. Iadarola, “Electron cloud studies for CERN particle accelerators and simulation code development,” CERN-THESIS-2014-047, University of Napoli, Italy (2014), <http://cdsweb.cern.ch/record/1705520>.

- [75] E. Skordis *et al.*, “FLUKA coupling to Sixtrack,” in Proc. ICFA Mini-Workshop on Tracking for Collimation, pp. 17–25, (2018), CERN Yellow Reports: Conference Proceedings, CERN-2018-011-CP, [doi:10.23732/CYRCP-2018-002](https://doi.org/10.23732/CYRCP-2018-002).
- [76] C. Boscolo Meneguolo *et al.*, “Study of beam-gas interaction at the LHC for the Physics Beyond Collider Fixed-Target study,” CERN-PBC-Notes-2019-001, <https://cds.cern.ch/record/2657636>.
- [77] E. Steffens and W. Haeberli, “Polarized gas targets,” *Rep. Prog. Phys.* **66** (2003) 1887, [doi:10.1088/0034-4885/66/11/R02](https://doi.org/10.1088/0034-4885/66/11/R02).
- [78] C. Boscolo Meneguolo, R. Bruce, M. Ferro-Luzzi, M. Giovannozzi and S. Redaelli, “Calculation of the allowed aperture for a gas storage cell in IP8,” (2018) CERN-PBC-Notes-2018-008, <https://cds.cern.ch/record/2651289>.
- [79] P. Di Nezza *et al.*, “The SMOG2 project,” (2018) CERN-PBC-Notes-2018-007, <https://cds.cern.ch/record/2651269>.
- [80] I. Bediaga *et al.* (LHCb Collaboration), “LHCb SMOG upgrade,” (2019) CERN-LHCC-2019-005; LHCb-TDR-020, <http://cds.cern.ch/record/2673690>.
- [81] B.K. Popovic, “VELO with SMOG2 impedance-based heating localization analysis,” (2019) CERN-PBC-Notes-2019-003, <https://cds.cern.ch/record/2666879>.
- [82] L. Mether *et al.*, “16L2: operation, observations and physics aspects,” in Proc. 8th Evian Workshop on LHC Beam Operation (2017), pp. 99–105, <https://cds.cern.ch/record/2654224>.
- [83] A. Lechner *et al.*, “Beam loss measurements for recurring fast loss events during 2017 LHC operation possibly caused by macroparticles,” in Proc. 9th Int. Particle Accelerator Conf. (IPAC2018), pp. 780–783, [doi:10.18429/JACoW-IPAC2018-TUPAF040](https://doi.org/10.18429/JACoW-IPAC2018-TUPAF040).
- [84] L. Mether, private communication. See also pres. at 14th meeting of the PBC FT working group, Wednesday 20 Feb 2019, [doi:10.5281/zenodo.3860067](https://doi.org/10.5281/zenodo.3860067).
- [85] P. Di Nezza *et al.*, “Internal gas target experiments at the LHC,” *PoS* **346** (SPIN2018) 011, [doi:10.22323/1.346.0011](https://doi.org/10.22323/1.346.0011).
- [86] E. Steffens *et al.*, “Design consideration on a polarized gas target for the LHC,” *PoS* **346** (SPIN2018) 098, [doi:10.22323/1.346.0098](https://doi.org/10.22323/1.346.0098).
- [87] L.L. Pappalardo *et al.*, The LHCSpin project, *PoS* **352** ((DIS2019) 233, [doi:10.22323/1.352.0233](https://doi.org/10.22323/1.352.0233).
- [88] E. Steffens, “Note on the efficiency of differential pumping in the LHC polarized gas target (PGT),” (2019) CERN-PBC-Notes-2019-002, <https://cds.cern.ch/record/2658197>.
- [89] E. Steffens, “Beam-induced depolarization and application to a polarized gas target in the LHC beam,” (2018) CERN-PBC-Notes-2018-001, <https://cds.cern.ch/record/2632904>.